Solid-State Crosslinkable, Shape-Memory Polyesters Serving Tissue Engineering

DOI: 10.1002/marc.202200955
Handle: http://hdl.handle.net/1942/39852

Solid-state crosslinkable, shape-memory polyesters serving tissue engineering

Jasper Delaey[1], Laurens Parmentier[1], Lincy Pyl[2], Joost Brancart[3], Peter Adriaensens[4], Agnes Dobos[1], Peter Dubruel[1], Sandra Van Vlierberghe[1,*]

[1]Polymer Chemistry & Biomaterials group (PBM), Centre of Macromolecular Chemistry (CMaC), Department of Organic and Macromolecular Chemistry, Ghent University, Ghent, Belgium
[2]Department of Mechanics of Materials and Constructions (MeMC), Vrije Universiteit Brussel (VUB), Brussels, Belgium
[3]Physical Chemistry and Polymer Science (FYSC), Vrije Universiteit Brussel, Brussels, Belgium
[4]Applied and Analytical Chemistry, Institute for Materials Research, Hasselt University, Diepenbeek, Belgium

[*]Corresponding author: Sandra.Vanvlierberghe@UGent.be

Keywords: Shape-memory, additive manufacturing, DLP, 2PP, polyester, polyurethane

1. Abstract

Acrylate-endcapped urethane-based precursors constituting a poly(D,L-lactide)/poly(ε-caprolactone) (PDLLA/PCL) random copolymer backbone were synthesized with linear and star-shaped architectures and various molar masses. It was shown that the glass transition and thus the actuation temperature could be tuned by varying the monomer content (0-8 wt% ε-caprolactone, $T_{g,crosslinked}$ = 10-42 °C) in the polymers. The resulting polymers were analyzed for their physico-chemical properties and viscoelastic behavior (G'_{max} = 9.6-750 kPa). The obtained polymers were subsequently crosslinked and their shape-memory properties were found to be excellent (R_r = 88-100%, R_f = 78-99.5%). Moreover, their potential towards processing via various additive manufacturing techniques (digital light processing (DLP), two-photon polymerization (2PP) and direct powder extrusion (DPE)) was evidenced with retention of their shape-memory effect. Additionally, all polymers were found to be biocompatible in direct contact *in vitro* cell assays using primary human foreskin fibroblasts (HFFs) through MTS assay (up to ~100% metabolic activity relative to TCP) and live/dead staining (> 70% viability).

2. Introduction

Shape-memory polymers (SMP) can actively change shape when exposed to a suitable trigger such as a change in temperature, hydration or exposure to certain wavelengths of light. Elastic energy can be stored in an arbitrary temporary shape through fixation of this shape (e.g. chemical crosslinking, crystallization, supramolecular interactions) and is released by changing back to a permanent shape upon application of a stimulus.[1] This type of polymers shows potential towards their use in the biomedical field where they can be employed in minimally

invasive surgery[2–4], drug release[5–7] or can allow for changes that would otherwise require manual intervention[8]. Two main types of thermo-responsive shape-memory polymers can be distinguished. The first type is based on physical crosslinking of a polymeric material, for example through crystalline regions which results in a thermoplastic material while the second type is based on chemical crosslinking and results in a thermoset. The latter possesses certain benefits such as thermal stability and solvent resistance along with superior shape fixation and recovery.[9] However, the former offers a superior range of processing options, while the processing options of the latter are not compatible with thermoplastic processing methods, such as direct powder extrusion 3D printing.

Tuning the transformation temperature at which thermoresponsive shape-memory polymers relax to their permanent shape (T_{trans}) near body temperature is generally considered as desirable for shape-memory polymers for intended use in biomedical applications. This enables the use of exposure to body temperature to trigger the shape-memory effect without the need for additional heat triggers which could potentially lead to cell damage.[10,11]

Shape-memory polymers based on either poly(D,L-lactide) (PDLLA) or poly(ε-caprolactone)(PCL)[9,12–14] have already been reported. For example, Zarek *et al.* employed a shape-memory polymer based on methacrylated PCL as an airway stent[9], while Yang *et al.* developed a copolymer of PDLLA and poly(trimethylene carbonate) which also exhibits shape-memory behavior.[13] Additionally, Fan *et al.* have reported on PLLA/PDLLA urethanes exhibiting excellent shape-memory properties with >99% fixity and recovery along with a fast shape recovery (within seconds). The recovery of their shape-memory polymer is based on the glass transition temperature (T_g) of the material, in the range of 38-46°C.[15] Xie *et al.* synthesized block copolymers of poly(lactide) (PLA) and poly(ethylene glycol) (PEG) to obtain physically crosslinked shape-memory polymers. Using urethane chemistry, they incorporated anthracene moieties, resulting in a light-inducible shape-memory effect in these materials based on the reversible photo-dimerization of the anthracene moieties (crosslinking and decrosslinking at λ >260 nm and <260 nm respectively).[16]

Lendlein and Langer reported on a physically crosslinked shape-memory polymer based on oligo(ε-caprolactone) diol segments as switching segments and oligo(p-dioxanone) diol as hard segments. They showed that this type of shape-memory polymer has potential to serve as degradable, self-tightening sutures when heated to 40°C.[17] Garle *et al.* synthesized a PCL-based shape-memory polymer by incorporating cinnamoyl moieties within their polymer to allow for chemical crosslinking. By controlling the way by which the cinnamoyl monomer was integrated in the polymer, being random or as a block-copolymer, and by controlling its content (0-100%) in the final polymer, they were also able to exert control over the melting temperature (T_m), which they exploited as a switch for the shape-memory polymer. More specifically, they recorded a T_m between 41 and 55 °C.[18] Also employing PCL and cinnamoyl groups, Wang *et al.* were able to obtain a triple shape-memory polymer. This material can be given two different temporary shapes for which the first transition is caused by the melting of the crystalline regions in the crosslinked polymer at 70 °C and the second by triggering the T_g of the polymer at 40 °C.[19]

However, while crystalline shape-memory polymers based on PLLA-PCL copolymers have been reported[20,21], no reports on random copolymers exploiting the amorphous variant of PLA, PDLLA, exist to date. This is remarkable since it has been shown that random copolymers of

poly(ε-caprolactone) and poly(D,L-lactide) allow for control of the glass transition temperature in the copolymer by varying the ratio of the constituting monomers.[22] The latter indicates that copolymerization of the corresponding monomers offers an excellent opportunity to tune the transition temperature T_{trans} of shape-memory polymers when exploiting the T_g as trigger. Additionally, by employing the amorphous variant of PLA, a transparent polymer can be obtained, providing interesting opportunities in the context of optical applications.

Acrylate-endcapped urethane-based precursors (AUP) are crosslinkable polymers with unique reactivity. They show an increased crosslinking reactivity in solid state.[23,24] Typically, this type of polymer is composed of a backbone to which a spacer group is attached through a diisocyanate. The spacer itself is endcapped with acrylate or methacrylate groups allowing for photo-crosslinking of the precursor material.[23]

In this study, the beneficial, solid-state crosslinking properties of AUPs are combined with the tunable glass transition temperature of a random PDLLA/PCL copolymer backbone to obtain a crosslinkable shape-memory polymer precursors that can be triggered at body temperature. We hypothesize that the resulting polymer will be biocompatible and can be processed by both extrusion and light-based additive manufacturing techniques and can be crosslinked in solid state to obtain the shape-memory material, resulting in extensive processing capabilities beyond those of conventional chemically crosslinked shape-memory materials. Additionally, the influence of the molar mass and backbone architecture on the shape-memory properties is studied.

3. Experimental

3.1. Materials

Ethyl acetate (≥99.5%, Sigma-Aldrich) was dried by overnight stirring with $MgSO_4$ (97%, anhydrous, Acros Organics). Toluene (p., Chem-Lab Analytical) and tetrahydrofuran (THF) (a.r., Chem-Lab Analytical) were refluxed with sodium metal (99.9%, Sigma-Aldrich) in the presence of benzophenone (>99%, Sigma-Aldrich) as an indicator before distillation. D,L-Lactide (99%, Sigma-Aldrich) was purified by recrystallization in dry ethyl acetate. ε-Caprolactone (97%, Sigma-Aldrich) was purified by vacuum distillation over CaH_2 (95%, Sigma-Aldrich). Ethylene glycol (≥99%, Acros Organics) and glycerol (99.6%, Acros Organics) were dried by fractioned vacuum distillation. Pentaerythritol (98%, Acros Organics) was dried by azeotropic distillation in dry toluene. $Sn(Oct)_2$ (Sigma-Aldrich), Bismuth neodecanoate (Umicore Specialty Materials), methanol (a.r., Chem-Lab Analytical), hexane (a.r., Chem-Lab analytical), disinfectol (Chem-Lab), Bisomer PEA6 (GEO specialty chemicals), triphenyl phosphate (TPP) (Fluka), phenothiazine (PTz) (Fluka), N-methyl-2-pyrrolidone (NMP) (≥99%, Sigma-Aldrich), isophorone diisocyanate (IPDI) (≥99%, Sigma-Aldrich), Irgacure 2959 (BASF), Speedcure TPO-L (Lambson), and Quinoline yellow (Sigma-Aldrich) were used as received. (2E,6E)-2,6-bis(4-(dimethylamino)benzylidene)-4-methylcyclohexanone (M2CMK) was synthesized as reported in literature.[25]

3.2. Synthesis

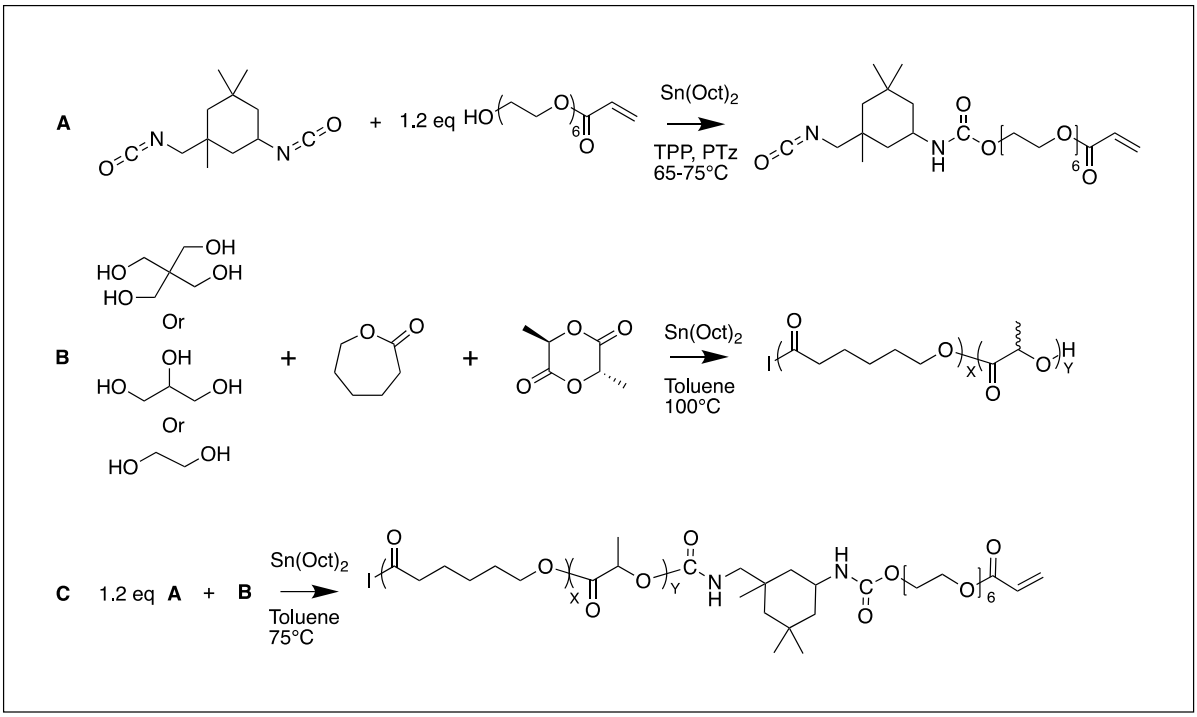

Figure 1. Synthesis scheme for the synthesis of A: AUP endcap, B: PDLLA/PCL random copolymer backbone and C: Reaction between the endcap and backbone to obtain a crosslinkable AUP polymer

3.2.1. Synthesis of the endcap

The applied endcapping reagent was synthesized from the reaction of Bisomer PEA6 with IPDI as shown in Figure 1A. IPDI (1eq) was mixed with 500 ppm TPP and 500 ppm PTz to the combined mass of the Bisomer and the IPDI, placed under Ar-atmosphere and heated to 65°C. Next, 1.2 equivalents of Bisomer PEA6 containing 500 ppm stannous octoate catalyst were added to the mixture in a dropwise fashion. The mixture was allowed to react for 2h before increasing the temperature to 75°C. After another 1h30 reaction time, the final product was obtained and stored at 5°C after cooling. The final product was used without further purification. LC-MS (Supplementary information, figure S1) analysis was performed on the endcap to asses the content of unreacted IPDI, it was found that only 2% of the endcap mixture contained unreacted IPDI while the remainder constituted the endcap reagent and the double reacted product.

3.2.2. Synthesis of crosslinkable polyester-urethanes

The synthesis route of linear, tri-, and four-armed PDLLA-PCL random block copolymers through ring-opening polymerization is depicted in Figure 1 B and C. Ethylene glycol, glycerol and pentaerythritol (1 eq) were used as initiators to obtain linear, tri-, and four-armed polymers respectively. D,L-Lactide and ε-caprolactone (CL) were mixed with dry toluene in a flame-dried Schlenk flask under inert atmosphere (Ar). The mixture was subjected to three freeze-pump-thaw cycles to remove residual oxygen and placed under Ar-atmosphere. The mixture was then heated to 100°C. Once complete dissolution of the monomers occurred, a mixture of the initiator and $Sn(Oct)_2$ (0.5 eq with respect to initiator OH) as catalyst in anhydrous toluene

was added to initiate the reaction. The solution was allowed to react for 24h after which the mixture was cooled down to 75 °C.
The endcap (1.2 eq, of the reactable endcap in the endcap mixture, as determined by LC/MS, with respect to initiator OH) was diluted with dry toluene (1:1 m V^{-1} %) and mixed with stannous octoate as catalyst (0.5 eq with respect to initiator OH). The endcap mixture was then injected in the polymerization solution in a dropwise fashion over the course of 20 min. The mixture was allowed to react overnight or until disappearance of the NCO-peak (~2264 cm^{-1}) in the FT-IR spectrum, after which the polymer was precipitated in a 10-fold excess of cold hexane (-20 °C). The precipitated polymer was dried *in vacuo* at 60 °C.
Further purification was performed by redissolving the polymer in acetone (1:2 w V^{-1} %) and adding an equal amount of double distilled water. Upon addition of water, a milky-white suspension was obtained. The suspension was then centrifuged (2000 RPM, 5 min) and the precipitate was collected. The filtrate was washed with double distilled water (half the volume of acetone used) and again centrifuged. The precipitated fractions were collected and dried *in vacuo* at 60 °C for 24h. After cooling, the resulting polymers formed a glassy, white-translucent solid.

3.2.3 Curing of the polymer

Cured films of the shape-memory polymers were obtained by dissolving the polymers in acetone (1:1 m V^{-1}) and adding Irgacure 2959 (2 mol% with respect to the acrylate functionalities) as photoinitiator. The solvent was then removed at a rotavapor, and the polymer was poured in a silicone mold between 2 glass plates covered by a Teflon release foil, the polymer was subsequently allowed to cool down to room temperature. The glass plates were exposed to UV-A irradiation (300-400 nm) from both sides (8 mW cm^{-2}) to obtain a crosslinked film.

3.3. Gel fraction and swelling degree experiments

Gel fractions were determined both in double distilled water and in acetone and performed in triplicate. Therefore, discs were punched out from dried crosslinked polymer (ø=8mm) sheets and incubated in 3 mL solvent in 6 well plates. The samples were then incubated for 3 days at 37 ℃. The gel fraction was calculated using equation 1 with m_d being the sample mass after incubation and drying and m_i the initial dry sample mass:

$$G(\%) = \frac{m_d}{m_i} \times 100\% \quad (1)$$

The degree of swelling was calculated using the following formula (2):

$$S(\%) = \frac{m_{sw} - m_d}{m_d} \times 100\% \quad (2)$$

With m_{sw} being the mass of the swollen sample.

Using the degree of swelling, the degree of crosslinking was approximated based on values available in literature for PLA using the Flory-Rehner equation (3) [26]:

$$\nu\ (\frac{mol}{mL}) = \frac{-[\ln(1-\nu_2) + \nu_2 + \chi\nu^2]}{V_s\left(\nu_2^{\frac{1}{3}} - \frac{\nu_2}{2}\right)}$$

(3)

With V_S the molar volume of the solvent and χ the polymer-solvent interaction parameter as defined by equation (4):

$$\chi = 0.34 + \frac{V_s}{RT}\left(\delta_{polymer} - \delta_{solvent}\right)^2$$

(4)

With $\delta_{polymer}$ and $\delta_{solvent}$ the solubility parameters of the polymer and the solvent respectively, R the gas constant and T the temperature in Kelvin.
Additionally, ν_2 represents the volume fraction of polymer in the swollen network and depends therefore on the degree of swelling (S) and density of the polymer ($\rho_{polymer}$) and solvent ($\rho_{solvent}$). It is calculated according to the following equation (5):

$$\nu_2 = \frac{1}{1 + \frac{S}{100\%} \cdot \left(\frac{\rho_{polymer}}{\rho_{solvent}}\right)}$$

(5)

3.4. Chemical Characterization

3.4.1. Nuclear magnetic resonance (NMR) spectroscopy

All ^{1}H-NMR spectra were recorded on a 400 MHz Bruker Avance II device. NMR spectra were analyzed using the MestReNova software package (version 12.0.4). NMR spectroscopy was applied for the determination of the molar mass of the polymer backbone (±10 mg in deuterated chloroform) before endcap modification using equation (6):

$$MW\left(\frac{g}{mol}\right) = I_{5.05-5.39\ ppm} \cdot \frac{MW_{Lactide}}{2} + \frac{I_{4-4.2\ ppm}}{n_{4-4.2\ ppm}} \cdot MW_{CL} + x \cdot \frac{MW_{Lactide}}{2} \cdot \left(1 - \frac{I_{3.64\ ppm}}{I_{4.23-4.5\ ppm} + I_{3.64\ ppm} - Y}\right) + x \cdot MW_{CL} \cdot \left(\frac{I_{3.64\ ppm}}{I_{4.23-4.5\ ppm} + I_{3.64\ ppm} - Y}\right) + MW_{initiator}$$

(6)

With $I_{5.05\text{-}5.39\ ppm}$ the integration of the peaks corresponding with the protons on the tertiary carbon of the lactide repeating units in the backbone, $I_{4\text{-}4.2\ ppm}$ the integration of the peaks characteristic for the protons on one of the secondary carbons of the CL repeating units in the backbone and $n_{4\text{-}4.2\ ppm}$ its corresponding number of protons (=2), $I_{3.64\ ppm}$ represents the integration of the signal corresponding with the protons on a terminal CL unit on a carbon next to the hydroxyl containing carbon. x represents the shape of the backbone and is 2, 3 or 4 when used with ethylene glycol, glycerol and pentaerythritol as initiator respectively. $I_{4.23\text{-}4.5\ ppm}$ represents the integration of the proton on the carbon next to the hydroxyl containing carbon of the terminal lactide unit of the PLA chains and is chosen as a reference peak for calibration of the spectrum and therefore defined as follows (equation (7)):

$$I_{4.23-4.5\ ppm} = Y + n(lactide) \cdot x$$

(7)

Here *n(lactide)* represents the molar fraction of lactide.
Since peaks characteristic for the initiator overlap with the terminal lactide peaks, *Y*, representing the overlapping protons of the initiator, is included in the calculations and is 4 for ethylene glycol and glycerol or 8 for pentaerythritol.

Acrylate contents of the synthesized AUP materials were calculated using dimethyl terephthalate as an internal standard. Therefore, around 10 mg of DMT and polymer were dissolved in deuterated chloroform (~750 µL). The acrylate content was then calculated using equation (8):

$$n(acrylates)\left(\frac{mol}{g}\right) = \frac{I_{6.4\ ppm} + I_{6.12\ ppm} + I_{5.83\ ppm}}{I_{8\ ppm}} \cdot \frac{n_{8\ ppm}}{n_{acrylates}} \cdot \frac{m(DMT)}{MW(DMT) \cdot m(polymer)} \quad (8)$$

With $I_{6.4\ ppm}$, $I_{6.12\ ppm}$ and $I_{5.83\ ppm}$ corresponding with the integrations of the protons of the acrylates, $n_{acrylates}$ represents the corresponding number of protons (=3), $I_{8\ ppm}$ is the integration of signal from the aromatic protons of DMT, $n_{8\ ppm}$ represents the number of corresponding protons (=4). *m(DMT)* and *m(polymer)* are respectively the masses of DMT and the polymer introduced in the NMR tube.

The degree of substitution was calculated using equation (9):

$$DS\ (\%) = \frac{I_{5.05-5.39\ ppm,\ backbone}}{I_{5.05-5.39\ ppm,\ AUP}} \times 100\% \quad (9)$$

Where the spectrum of the backbone is calibrated according to equation (8) and the spectrum of the AUP is calibrated using the acrylate peaks where their integration is given by the amount of acrylate protons per acrylate group (3) multiplied with the number of arms in the polymer (2, 3 and 4 for ethylene glycol, glycerol and pentaerythritol as initiator respectively).

High resolution magic angle spinning (HR-MAS) ^{1}H-NMR spectroscopy was used to determine the absolute degree of crosslinking (DC) of the polymers. In this regard, NMR spectra of the initial materials were taken before crosslinking using conventional ^{1}H-NMR spectroscopy while HR-MAS NMR spectroscopy was used to obtain the spectra of crosslinked samples. To this end, around 10 mg of crosslinked sample was swollen in deuterated chloroform (~40-60 µL) in a Kel-F disposable insert and placed in a zirconium HR-MAS rotor closed with a Kel-F cap. The sample was measured in a Bruker Avance II 700 spectrometer at a spinning rate of 6 kHz. The degree of crosslinking was then calculated using the following equation (10):

$$DC(\%) = \frac{\frac{I_i}{I_{ri}} - \frac{I_e}{I_{re}}}{\frac{I_i}{I_{ri}}} \times 100\% \quad (10)$$

With I_i and I_{ri} the integrations of respectively the acrylate peaks and the reference peak before crosslinking and I_e and I_{re} the integrations of respectively the acrylate peaks and the reference

peak after crosslinking. Herein, the peak at 2.25 ppm was chosen as a reference peak since it does not change during the crosslinking reaction.

3.4.2 FT-IR

FT-IR analysis was performed using a Frontier FT-IR/FIR spectrometer.

3.4.3 DMA

DMA was performed on a Q800 device by T.A. Instruments, with the sample being mounted in tensile mode. Shape-memory properties were determined according to a controlled force procedure based on a whitepaper published by TA-instruments.[27] The sample was stretched at 0.1 N min^{-1} to a maximum stress of 0.05 N at 40 °C. The sample was then cooled down to -10 °C (T_{low}) and kept isothermal for 10 min. The force was then released, and the sample was kept isothermal for another 10 min. The sample was reheated to 40 °C (T_{high}) using a 5 °C min^{-1} temperature ramp, after which the sample was kept isothermal for 45 min. This procedure was repeated 4 times for a total of 5 cycles. Results were analyzed using the Advantage/Universal analysis software package.
Shape fixity (R_f) and shape recovery (R_r) were calculated using equations (11) and (12) respectively[28]:

$$R_f(N) = \frac{\varepsilon_u(N)}{\varepsilon_l(N)} \times 100\% \quad (11)$$

$$R_r(N) = \frac{\varepsilon_l(N) - \varepsilon_p(N)}{\varepsilon_l(N) - \varepsilon_p(N-1)} \times 100\% \quad (12)$$

With $\varepsilon_l(N)$ the maximum strain in cycle N, $\varepsilon_u(N)$ the strain after unloading and cooling to T_{low}, $\varepsilon_p(N)$ the remaining strain of the recovered shape in cycle N and $\varepsilon_p(N-1)$ the remaining strain after recovery of cycle N-1.

3.4.4 Photorheology

Photorheological measurements were conducted on an Anton Paar MCR 302e rheometer. To this end, the polymers were dissolved in acetone (100 m V^{-1} %) with 2 mol% Irgacure 2959 added as photoinitiator with respect to the acrylate functionalities. 250 µL was dispensed on a transparent bottom plate after which the spindle ($\emptyset$=25 mm) was lowered to a gap of 0.3 mm. Plateau values for the storage (G') and loss (G'') moduli were calculated by averaging the data after 15 minutes of measurement, since at this point, all polymers had reached their plateau values. Amplitude and frequency sweeps were performed prior to measuring to determine the linear visco-elastic region. An amplitude of 1% and a frequency of 1 Hz were selected. After 3 min, the UV-light source (OmniCure series 1500) using a 320-480 nm filter was switched on for 30 min at an intensity of 100 mW cm^{-2} at the position of the material. Measurements were performed at 25°C in triplicate.

3.4.5 Accelerated in vitro degradation assay

Accelerated hydrolytic degradation was monitored on selected samples. To this end, samples were solvent-casted and crosslinked as described earlier (section 3.2.3). Disks ($\emptyset$ = 4mm)

were punched out of the obtained sheet and incubated in a 1M NaOH (48 well plate, ±1 ml/well) solution at 37 °C. Initial sample mass was noted and samples were taken out of the well plate periodically, followed by drying *in vacuo*. The mass of the dried samples was determined relative to the initial mass to obtain the degradation curves. All measurements were performed in triplicate.

3.5. Thermal Characterization

3.5.1. Thermogravimetric analysis (TGA)

Thermal degradation properties of the PDLLA/PCL copolymers and the AUP were studied using thermogravimetric analysis using a TA instruments Q50 device under N_2 atmosphere. A heating ramp of 10 °C min^{-1} was used to a maximum temperature of 600 °C. Results were analyzed using the Advantage/Universal analysis software package. As degradation points the degradation onset ($T_{d,onset}$) and the maximum of the first derivative ($T_{d,max}$) were taken.

3.5.2. Differential scanning calorimetry (DSC)

Thermal transitions were characterized using differential scanning calorimetry using a TA instruments Q2000 device. Results were analyzed using the Advantage/Universal analysis software package. A heating ramp of 10 °C min^{-1} to 120 °C and a cooling ramp of 5 °C min^{-1} to -50 °C were used. About 5-10 mg of polymer sample were subjected to a heating cycle followed by a cooling cycle and a second heating cycle.

3.6. In vitro biological characterization

The cytocompatibility of the various materials was evaluated according to the ISO-10993 standard. Culture medium of the primary human foreskin fibroblasts (HFFs) consisted of Dulbecco's Modified Eagle Medium (DMEM) containing 10 v v^{-1} % Fetal Bovine Serum (FBS) and 1 v v^{-1} % penicillin/streptomycin. Refreshment of the culture medium was performed twice a week with sub-culturing after reaching 80-90% confluency. Standard incubator conditions (37°C, 5% CO_2) were used. Punched out disks (Ø = 6 mm) from photo-crosslinked sheets were sterilized with 70 v v^{-1} % EtOH for 24 h with a change after 12 h followed by UV-C irradiation (100-280 nm, 15 mW cm^{-2}) for 2 hours. HFFs were used at passage number 14 and seeded at a density of 10,000 cells per well in a 96-well plate. After one day, the sterilized materials were placed in contact with the seeded monolayer. Cytocompatibility was then evaluated in terms of viability (live/dead assay) and metabolic activity (MTS assay) after 1, 3 and 7 days.

3.6.1 Live/dead assay

After the addition of Ca-AM (0.2 v v^{-1} %) and Propidium Iodide (0.2 v v^{-1} %) in PBS to the cells and 15 minutes of incubation in the dark, the viability (living green cells/total amount of cells including red dead cells) could be verified with fluorescence microscopy using an Olympus IX 81 with Xcellence Pro software together with a green fluorescent protein (GFP) filter and a Texas Red (TxRed) filter. FIJI software (version 2.3.0) was used to compute the percentage viability where viability was defined as the ratio of live cells over the total cell count. All samples were analyzed in triplicate.

3.6.2. MTS assay

The MTS assay was used to assess the metabolic activity through the bioreduction of the tetrazolium compound into formazan. 16 v v^{-1} % MTS in culture medium was added to the monolayer of cells and incubated in the dark (37°C, 2h) under continuous shaking. The absorbance maximum of the formazan product was measured at 490 nm using an EL800 Universal Microplate Reader (BioTek Instruments) with Gen5 software. All samples were analyzed in triplicate.

3.6.3. Statistics

Statistical analysis was performed using two-way ANOVA using the Prism 8 software by GraphPad (version 8.3.1).

3.7. Processing using additive manufacturing techniques

3.7.1. Digital light processing (DLP)

Printing was performed on a LumenX DLP-printer from Cellink. To this end, 1 mL of resin was dispensed in the resin vat. Vertical resolution was set to 100 μm and layers were illuminated for 2s, using twice the illumination time for the initial layers. The printer light source intensity was set to 50% (33 mW/cm^2). The resulting print was then dipped in disinfectol and excess resin from the print was carefully removed. To remove the solvent present in the print, the print was placed in a bath of demineralized water for 2 hours followed by a 1 hour drying cycle at 100 ℃.

3.7.2. Two photon polymerization (2PP)

Printing was performed in solid-state using a NanoOne BIO 2PP device from UpNano. The polymer was dissolved in acetone (66 m V^{-1} %) in the presence of TPO-L or M2CMK[25,29] as photoinitiator at a 5wt% (~18 mol%) and 1wt% (~10 mol%) concentration respectively. A droplet of the solution was then placed on a methacrylated glass slide and the solvent was evaporated at 40 °C. Writing speeds of 100-600 mm s^{-1} and a laser power of 90 mW were used. After printing, uncured resin was washed away using two washing steps in N-methyl-2-pyrrolidone (NMP).

3.7.3. Direct powder extrusion (DPE)

Printing was performed using a BIO V1 printer by Regemat. Herefore, polymer powder blended containing 2 mol% of Irgacure 2959 was loaded in the thermoplastic accessory. A 19-gauge needle was used to extrude the polymer directly onto the build plate. Extrusion parameters can be found in Table 6. After printing, the construct was crosslinked by irradiating the construct with UV-A irradiation (300-400 nm) from both sides (8 mW/cm^2).

4. Results and Discussion

4.1. Synthesis and characterization of AUP-polyesters.

Acrylate-endcapped urethane-based precursors (AUP)-polyesters were synthesized by first conducting a ring opening polymerization of D,L-Lactide and ε-caprolactone using various

initiators. These monomers were selected to yield an amorphous and biodegradable backbone material while the modification towards an AUP material will ensure the solid state crosslinkability, as previously reported.[23] ε-caprolactone was included to reduce the glass transition temperature (T_g) of PDLLA (55-60 °C[30]) below body temperature, therefore ε-caprolactone contents of 6 and 8% (~7.5 and 10 mol% respectively) were selected since these concentrations are hypothesized to yield polymers with at T_g between body temperature and room temperature, based on Fox' equation, enabling effective triggering of the shape-memory effect in *in vivo* conditions. Ethylene glycol was used as an initiator to obtain linear polymers while glycerol and pentaerythritol were used to obtain star-shaped polymers with 3 and 4 arms, respectively. These polyesters were then endcapped by reacting the terminal hydroxyl functionalities with a diisocyanate constituting an oligomeric ethylene glycol spacer and a terminal acrylate functionality. By using star-shaped polymers, the acrylate content can be increased for polymers with similar molar mass compared to their linear counterparts. Moreover, it has been shown that star-shaped polymers have lower viscosities than their linear counterparts, potentially facilitating deposition-based 3D-printing.[31,32] The molar mass of the polymers was varied by adjusting the initiator:monomer ratio. The molar mass of the target polyesters was determined using ^{1}H-NMR spectroscopy. A naming convention according to the following formula was adopted for the polymers:

n-PDLLA/PCLx-yK-AUP

Here, *n* indicates the multiplicity of the initiator and thus the number of arms, *x* indicates the PCL content in the polymer in wt%, if no PCL is included in the polymer only PDLLA is mentioned in the naming convention, *yK* indicates the molar mass of the backbone unit in the polymer (e.g. 8K indicates a backbone mass of ~8000 g/mol), finally *AUP* indicates that the backbone has been modified with a spaced, acrylated endcap, resulting in a AUP-type polymer.

Additionally, the acrylate content after endcapping was determined against an internal standard (Table 1). An example of a representative ^{1}H-NMR spectrum of an AUP material is shown in Figure 2.

Table 1. Overview of the synthesized AUP materials

Material	CL content [wt%]	Initiator	Architecture	$M_{n,\ NMR}$ [g mol^{-1}]	Acrylate content [mmol g^{-1}]	DS [%]
2-PDLLA/PCL6-11K-AUP	6	Ethylene glycol	Linear	11390	0.12	52
2-PDLLA/PCL6-4K-AUP	6	Ethylene glycol	Linear	4360	0.46	93
2-PDLLA/PCL6-7K-AUP	6	Ethylene glycol	Linear	7340	0.23	84
2-PDLLA/PCL6-9K-AUP	6	Ethylene glycol	Linear	8780	0.29	100
2-PDLLA/PCL8-8K-AUP	8	Ethylene glycol	Linear	8430	0.30	88
3-PDLLA-9K-AUP	0	Glycerol	Star: 3-armed	9340	0.33	92
4-PDLLA-12K-AUP	0	Pentaerythritol	Star: 4-armed	11890	0.34	73
4-PDLLA/PCL6-2K-AUP	6	Pentaerythritol	Star: 4-armed	1950	0.91	92

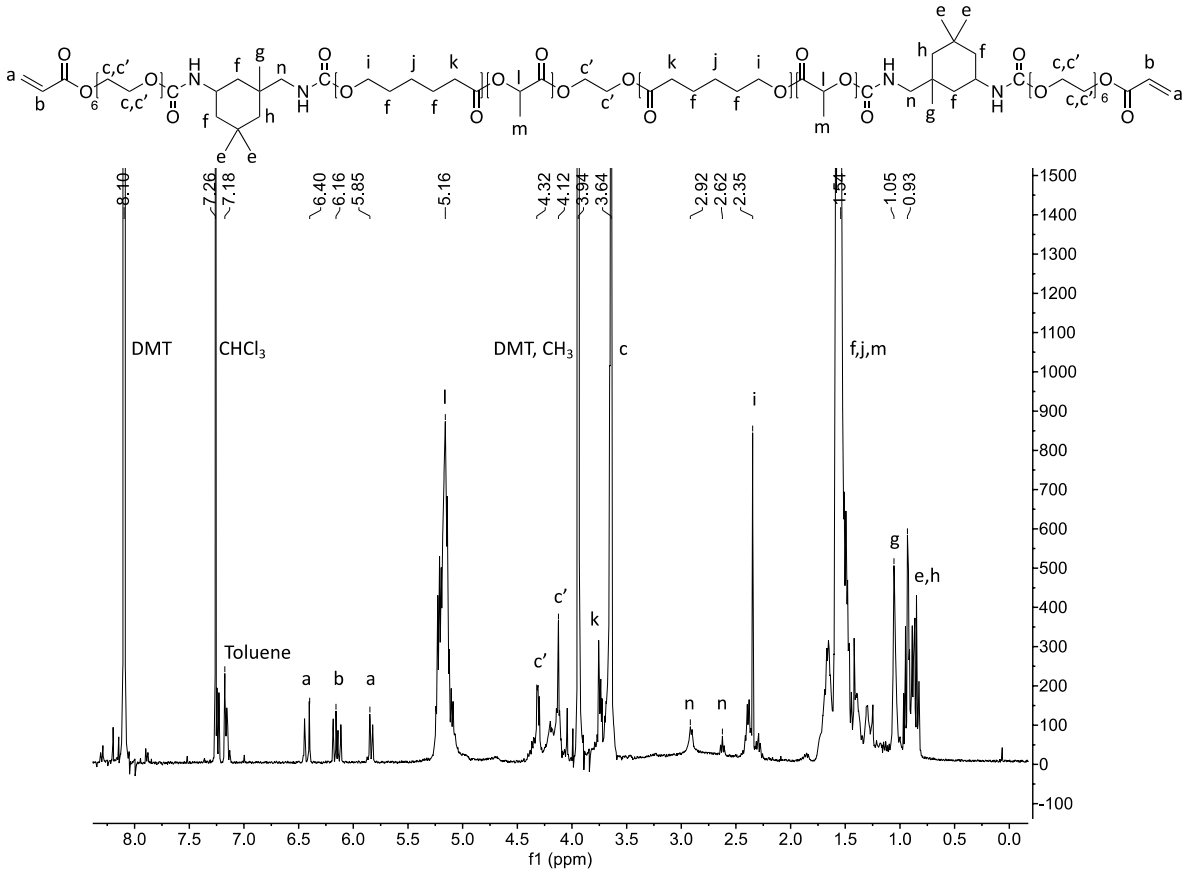

Figure 2. Assigned ^{1}H-NMR spectrum of 2-PDLLA/PCL8-8K-AUP in the presence of DMT as an internal standard with all peaks assigned.

Analysis of the FTIR spectra of the endcap before modification and the endcapped polymer show a disappearance of the -NCO peak at 2260 cm^{-1}, indicating successful modification of the polyester. This is also confirmed by the increase of the peak around 3380 cm^{-1} which is indicative for the N-H stretch and indicates the formation of a urethane bond. Additionally, the strong C=O peak at 1750 cm^{-1} indicates the presence of the polyester backbone. Moreover, both polyester peaks (δ = 5.16, 2.35, 1.54 ppm) and acrylate peaks (δ = 6.4, 6.12 and 5.83 ppm) are also present in the ^{1}H-NMR spectrum of the purified polymer, indicating the successful modification of the polymer (Figure 2).

When comparing the FTIR-spectra before and after crosslinking, no notable changes are visible except a considerable increase of the peak around 3400 cm^{-1}, this increase can be attributed to the -OH group of the initiator used for crosslinking (Irgacure 2959).

As expected, when comparing acrylate content with molar mass per arm of the polymer, where a linear polymer is considered to be a star shaped polymer with two arms, a clear linear relationship can be found where increasing molar mass results in lower acrylate content.

4.2. Characterization of the polymer networks

The crosslinked networks were analyzed using HR-MAS ^{1}H-NMR spectroscopy to determine the degree of crosslinking. Additionally, gel fraction (G%) and swelling degree (S%) values were determined in both water and acetone and are reported in Table 2. In acetone, the crosslink

density (ν) of the network was also estimated based on parameters available for PLA and are reported in Table 2.

Table 2. Overview of swelling degrees (S) and gel fractions (G) of the AUP materials in both water and acetone. (n=3)

Material	G, H_2O [%]	S, H_2O [%]	G, Acetone [%]	S, Acetone [%]	$\nu \times 10^5$ [mol mL^{-1}]	DC [%]	Acrylate content [mmol g^{-1}]
2-PDLLA/PCL6-11K-AUP	89.48 ± 0.38	92.16 ± 15.80	21.32 ± 3.76	1852.66 ± 94.62	0.32 ± 0.03	78	0.12
2-PDLLA/PCL6-4K-AUP	89.94 ± 1.79	2.12 ± 1.72	79.57 ± 0.73	505.57 ± 45.61	3.13 ± 0.46	100	0.46
2-PDLLA/PCL6-7K-AUP	88.99 ± 0.44	62.08 ± 4.16	17.74 ± 6.06	1156.87 ± 63.34	0.75 ± 0.03	79	0.23
2-PDLLA/PCL6-9K-AUP	90.46 ± 0.34	17.44 ± 1.56	81.53 ± 1.24	831.46 ± 38.26	1.29 ± 0.10	99	0.29
2-PDLLA/PCL8-8K-AUP	91.12 ± 0.16	93.74 ± 5.92	44.79 ± 8.43	439.45 ± 1.64	2.76 ± 0.01	15	0.30
3-PDLLA-9K-AUP	91.34 ± 0.69	10.73 ± 0.77	60.66 ± 0.32	686.90 ± 25.88	1.76 ± 0.05	92	0.33
4-PDLLA-12K-AUP	88.17 ± 3.84	37.03 ± 5.65	47.85 ± 7.86	1218.61 ± 58.5	0.64 ± 0.02	19	0.34
4-PDLLA/PCL6-2K-AUP	90.60 ± 0.26	5.89 ± 6.01	98.46 ± 0.98	303.84 ± 85.83	8.51 ± 3.53	100	0.91

Noticeable are the relatively low gel fractions of 2-PDLLA/PCL6-7K-AUP and 2-PDLLA/PCL6-11K-AUP in acetone, albeit not unsurprising given that these polymers have the lowest acrylate content of all synthesized polymers. 4-PDLLA/PCL6-2K-AUP on the other hand has the highest acrylate content and will thus result in the most densely crosslinked network as also indicated by the network density ($8.51 \pm 3.53 \times 10^{-5}$ mol mL^{-1}). Furthermore, this network is characterized by the lowest swelling degree and the highest gel fraction. Noticeable is the fact that the gel fraction in H_2O is lower than the gel fraction in acetone for this polymer. A plausible explanation for this might be the hydrolytic degradation of the polymer network causing leaching of lactic acid. This was corroborated by the continuously dropping pH value of the swelling medium (supplementary information, Figure S59).
Additionally, when comparing network densities with acrylate contents, there exists a clear correlation, with rising acrylate content resulting in denser networks. This was anticipated since

acrylates will form the crosslinks in the network. Consequently, since the latter is correlated with the molar mass per polymer arm, the network density is also correlated with the molar mass per polymer arm with higher molar masses resulting in lower densities. This behavior is in line with the expectations since assuming 100% crosslinking, the molar mass of a polymer arm will be equal to the molar mass between crosslinks (M_c), which is correlated with the swelling and thus the crosslink density according to the Flory-Rehner equation.[33]
When considering the degree of crosslinking, it can be noticed that most polymers show a high degree of crosslinking (>75% conversion of the acrylates) with two exceptions, namely 2-PDLLA/PCL8-8K-AUP and 4-PDLLA-12K-AUP which show DC's of 15% and 19% respectively. These lower conversions might be related to the relatively high molar mass of the polymers which spaces the acrylates further apart. Interestingly, this can explain the relatively low gel fractions in acetone (44.79% and 47.85% respectively) of these polymers, since less conversion will mean that less polymer strands are incorporated in the network, resulting in a higher leachable fraction.

4.3. Thermal properties of the AUPs before and after crosslinking

The thermal properties of the AUPs were assessed using DSC and TGA. All recorded values of the thermal transitions can be found in Table 3. The TGA and DSC graphs can be found in the supplementary information. Since all materials make use of D,L-lactide as a monomer with random incorporation of CL segments rather than block-co-polymerization, the backbones are amorphous. Even after modification, no crystallization or melting peaks could be observed in the DSC thermograms, indicating that all polymers are indeed amorphous.
Additionally, incorporation of CL in the polymer allows for tuning of the glass transition temperature of the backbone which is needed to obtain a T_g between body and room temperature, enabling triggering of the shape-memory effect at physiological conditions. Triggering of the shape-memory effect due to physiological conditions is interesting as there is no need for external heating. An example of a potential application includes cardiovascular stents where the stent is protected by a sheath until reaching the target location, after which the sheath can be removed and the shape-memory stent can unfold.[34] This is also clear from the glass transition temperature of 3-PDLLA-9K-AUP and 4-PDLLA-12K-AUP, where no CL is incorporated in the chains, with a T_g in the crosslinked state of 42 °C and 40 °C, respectively. Since both polymers show a T_g above body temperature, they are therefore not suited as shape-memory materials to be triggered at body temperature. Polymers incorporating CL, on the other hand, show a T_g below body temperature. 2-PDLLA/PCL8-8K-AUP, which contains 8 wt% CL in the backbone, even has a T_g of 27 °C. However, it can be argued that this T_g is too low since the onset of the T_g already starts around 22 °C, which is too close to room temperature, hence having the risk of triggering the shape-memory effect before implantation. Therefore, the incorporation of 6 wt% CL is considered ideal to obtain a shape-memory AUP that can be triggered between room temperature and body temperature. This resulted in a T_g of 29 to 35 °C, depending on the Mn of the resulting AUP (Table 3).

Moreover, when considering the glass transition temperatures after crosslinking of the polymers, the values can be fitted to Fox' equation, as can be seen in Figure 3. The variation

between the T_g values of polymers with the same composition is most likely linked to differences in molar mass of the polymers rather than the influence of the endcaps. This is especially clear when comparing 4-PDLLA/PCL6-2K-AUP with other polymers of equal CL content. Based on the relatively high spacer content in this polymer, it would be expected that, if the spacer would have a significant influence on the glass transition temperature of the crosslinked polymer, the glass transition temperature of this polymer would be substantially lower. However, the opposite observed. It is therefore hypothesized that this is related to the restrict chain mobility due to crosslinking, which will be most noticeable at the terminal groups of the polymer where the ethylene glycol spacer is located. This is also evidenced by the fact that there exists a larger difference in T_g between uncrosslinked and crosslinked material in polymers with a larger endcap content and that independent of endcap content, the T_g after crosslinking always rises to values that would be expected based solely on the backbone composition. Therefore, the glass transition temperature of the crosslinked polymer can easily be predicted by employing Fox' equation based on the composition of the polymer backbone, hence facilitating the design of a polymer exhibiting the desired glass transition temperature. It should be noted that there will also be an effect of the molar mass on the T_g of the materials. However, this effect will be negligible compared to the effect of the PEG spacer.

Table 3. Glass transition temperatures of the crosslinked and uncrosslinked materials and thermal degradation temperatures.

Material	$T_{g,uncrosslinked}$ [°C]	$T_{g,\ crosslinked}$ [°C]	ΔT [°C]	$T_{d,\ onset}$ [°C]	$T_{d,\ max}$ [°C]
2-PDLLA/PCL6-11K-AUP	26.3	37.8	11.5	211.5	236.7
2-PDLLA/PCL6-4K-AUP	0.0	29.0	29.0	201.4	245.5
2-PDLLA/PCL6-7K-AUP	23.0	33.7	10.7	217.8	250.9
2-PDLLA/PCL6-9K-AUP	16.9	34.9	17.9	209.4	230.4
2-PDLLA/PCL8-8K-AUP	5.5	27.3	21.8	213.0	253.2
3-PDLLA-9K-AUP	16.3	42.4	26.0	247.1	259.6
4-PDLLA-12K-AUP	24.3	40.0	15.6	210.5	233.3
4-PDLLA/PCL6-2K-AUP	-13.9	33.9	47.8	226.6	291.3

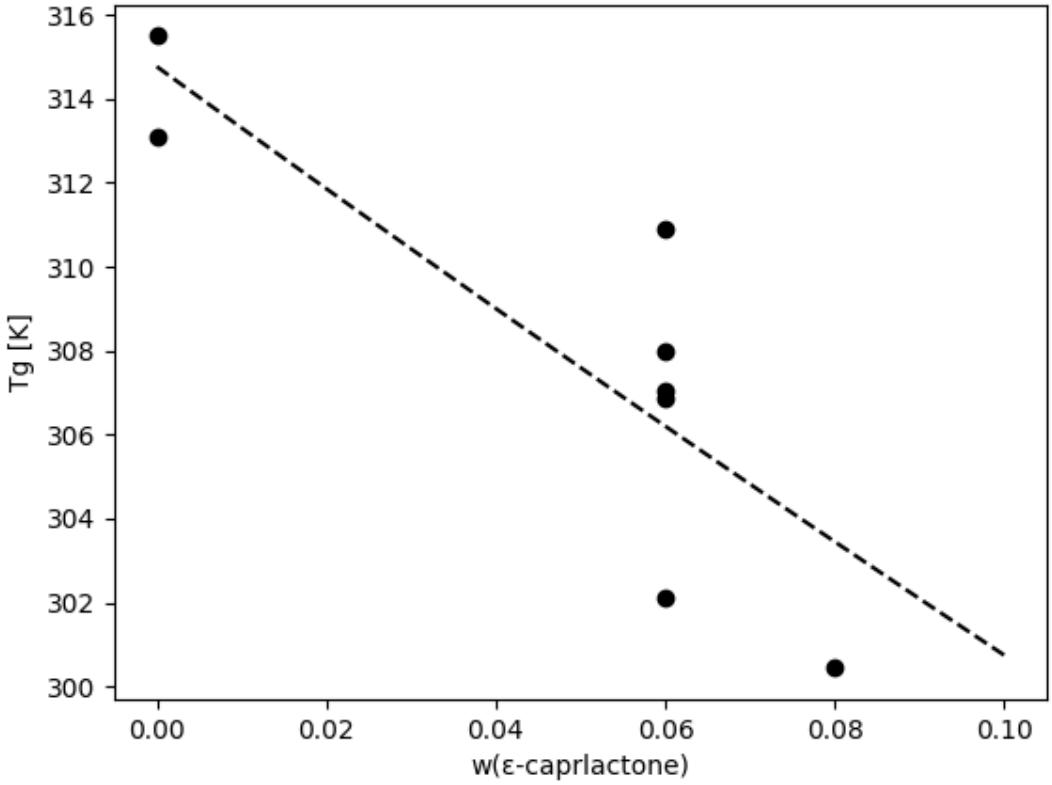

Figure 3. Fit of polymer glass transition temperature after crosslinking to the Fox' equation.

4.4. Photorheology of the AUP's

Photorheology was performed on the samples in a 100% m V^{-1} concentration in acetone to reduce the viscosity which results in conditions more similar as those employed in DLP printing where viscosity below 3 Pa.s is desired.[35] An example of a curve obtained by photorheology is displayed in Figure 4, other curves are shown in the supplementary information.

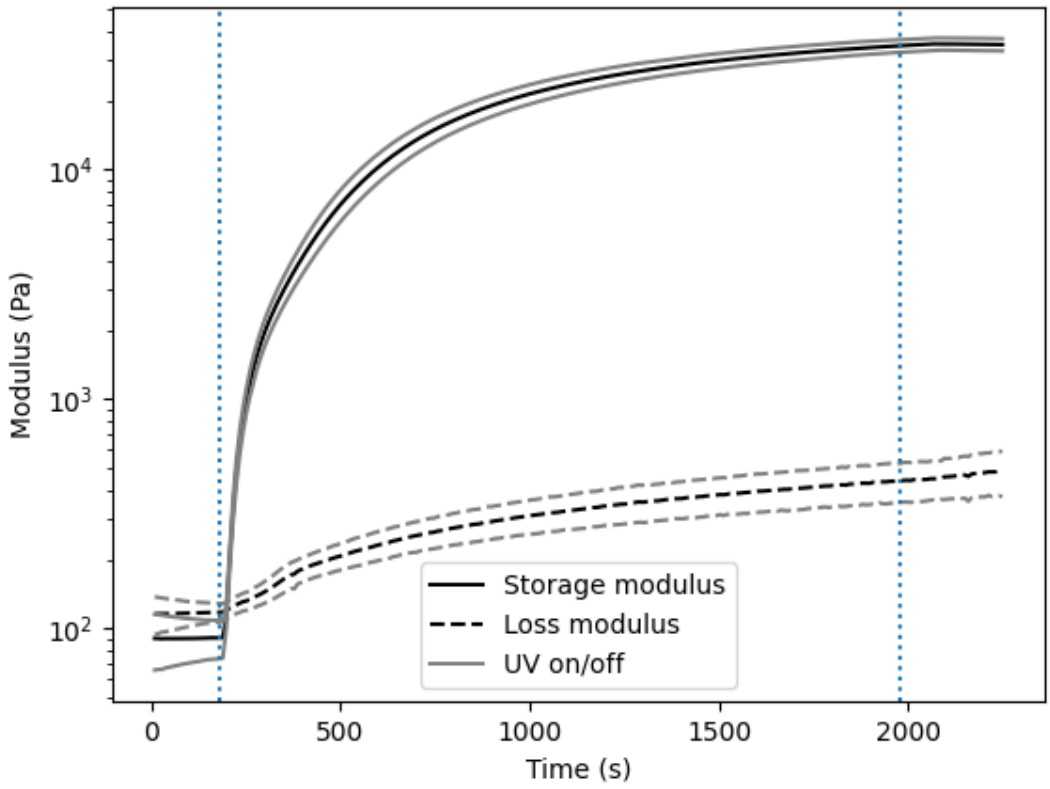

Figure 4: Example of photorheology measurement for 2-PDLLA/PCL6-9K-AUP, The dotted blue lines indicate the timepoints at which the UV irradiation is turned on and off. The light gray lines represent the standard deviation on the measurement (n=3).

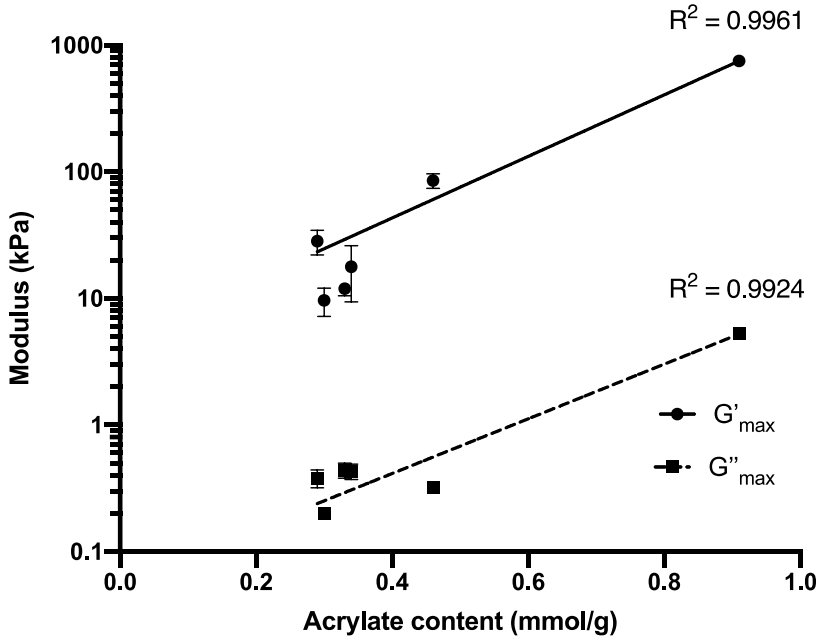

Figure 5. Relationship between the loss/storage modulus and the acrylate content of the polymers. Note the logarithmic nature of the y-axis.

When considering the storage modulus and loss modulus plateau values for the polymers after crosslinking (Table 4), an exponential relationship exists between the storage and loss modulus with respect to the acrylate content (Figure 5). This allows for the prediction of the properties of the materials based solely on the measured acrylate content. The higher moduli for polymers with a higher acrylate content is related to the fact that polymers with a higher acrylate content will form more densely crosslinked networks. Similar relationships between these moduli and the crosslink density have been reported in literature.[36–38] When considering the time points at which these values are reached, a similar trend was observed. Polymers containing more acrylates will crosslink faster, since a higher number of acrylates will be present in each volume unit. Therefore, reaction between two acrylates is more likely to occur in polymers with a lower molar mass per arm and hence, a higher acrylate concentration results in a higher rate of polymerization. This is in line with expectations for free radical polymerizations, where the rate of polymerization shows a linear correlation with the monomer concentration.[39]
Two polymers did not crosslink, namely 2-PDLLA/PCL6-7K-AUP and 2-PDLLA/PCL6-11K-AUP. However, these two polymers are also those exhibiting the lowest acrylate content (0.23 and 0.12 mmol g^{-1} respectively). Therefore, it is reasonable to assume that given the dilution of the samples, which was performed to simulate DLP like conditions, for rheological measurement, the acrylate concentration became too low to allow for efficient crosslinking resulting in network formation. When crosslinked in solid state on the other hand, which was done to prepare samples for determination of the shape-memory properties using DMA and for the determination of the swelling degree and gel fraction, crosslinking did take place. This is evident from the fact that no complete dissolution of the polymers occurred when incubated in acetone for the determination of the gel fraction, while uncrosslinked polymers dissolved completely, and from the fact that it was possible to determine a gel fraction at all. Another reason for this could be the superior solid-state crosslinking of AUP materials which allow crosslinking of the shape-memory precursors to crosslink more effectively in solid state than in solution.[23,24]

Table 4. Storage and loss moduli of the crosslinked materials (n=3)

Material	G'_{max} [kPa]	G''_{max} [kPa]
2-PDLLA/PCL6-11K-AUP	No crosslinking	No crosslinking
2-PDLLA/PCL6-4K-AUP	85.3 ± 11.3	0.32 ± 0.03
2-PDLLA/PCL6-7K-AUP	No crosslinking	No crosslinking
2-PDLLA/PCL6-9K-AUP	28.3 ± 6.2	0.38 ± 0.06
2-PDLLA/PCL8-8K-AUP	9.6 ± 2.4	0.20 ± 0.02
3-PDLLA-9K-AUP	11.9 ± 1.4	0.44 ± 0.06
4-PDLLA-12K-AUP	17.7 ± 8.4	0.43 ± 0.06
4-PDLLA/PCL6-2K-AUP	749.9 ± 11.3	5.23 ± 0.15

4.5. Shape-memory effects

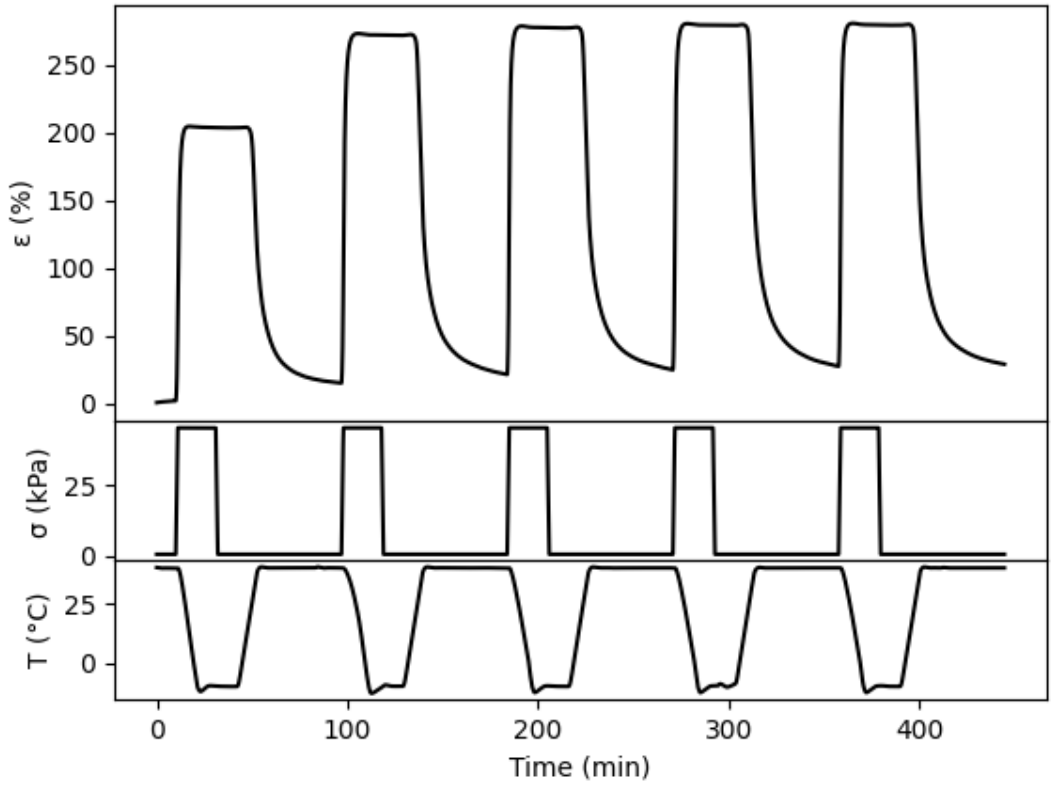

Figure 6. Example of data recorded by the cyclic thermomechanical analysis of 2-PDLLA/PCL6-11K-AUP. The strain and temperature show the conditions during the programming (max stress and T_{max} to T_{min}) and recovery (T_{max} and 0 stress). The strain response shows the deformation due to programming and the recovery of the original shape upon heating. The deviation in cycle 1 can be explained by the fact that it is a preconditioning to remove the thermomechanical history.

The performance of shape-memory polymers is evaluated based on how well the programmed shape is fixed into the polymer structure and retained over time and based on the extent to which the original shape is recovered. To determine the shape fixity (R_f) and the shape recovery (R_r) properties, cyclic thermomechanical testing was performed using DMA. A typical test procedure is shown in Figure 5 and the results of these tests are summarized in Table 5. During the first cycle the thermal and mechanical history of the sample is erased by a conditioning step. In the present work, chemically crosslinked amorphous polymers were used in which vitrification acts to fix the temporary shape of the network. Heating the polymers above their glass transition temperature resulted in the recovery of the permanent shape. All materials show excellent shape fixity properties already in the first cycle with no substantial change in later cycles. The relatively inferior performance of 2-PDLLA/PCL6-9K-AUP could be explained by the limited strain at the applied force in this sample, resulting in incomplete preconditioning and the incomplete removal of the thermomechanical history of the sample. The shape recovery on the other hand improves with the number of cycles. Especially the first cycle is an outlier here. However, this was anticipated since the first cycle is generally used to erase the thermal history of the sample and similar trends are observed with other shape-memory polymers.[28]

Eventually, all materials reach excellent recovery values in cycle 3, with a marginal improvement by cycle 5, in which most materials approach 100% recovery.

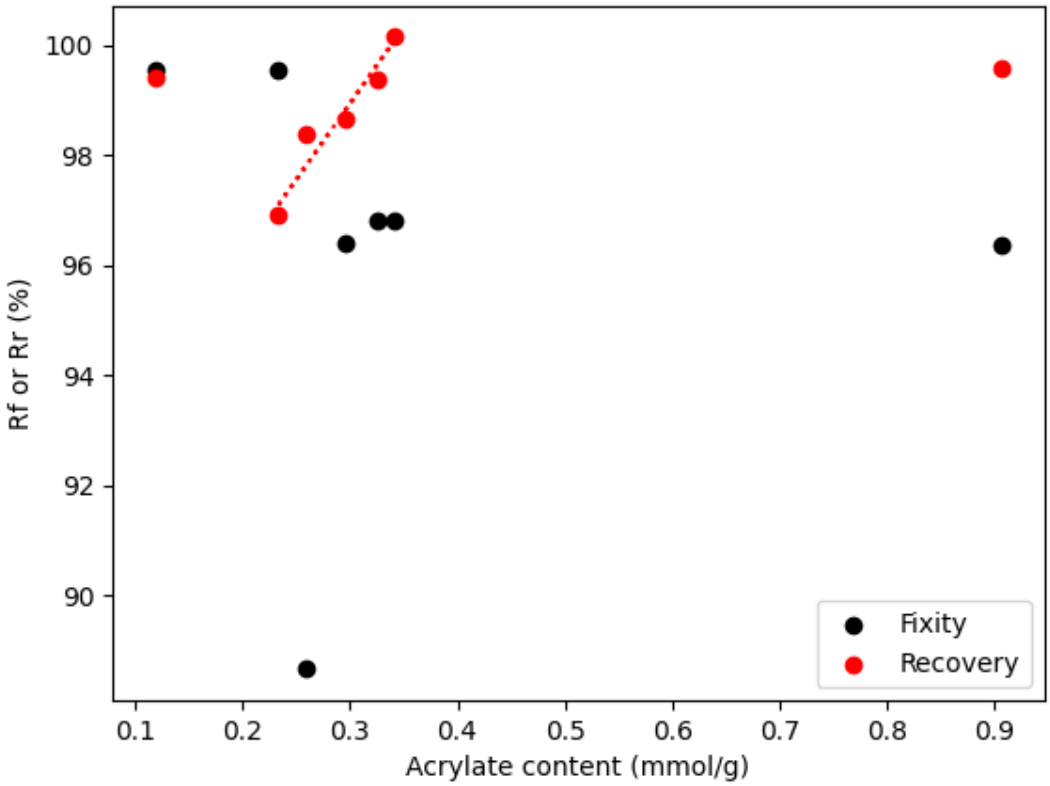

Figure 7. Relation between shape-memory properties in cycle 5 and acrylate density of the polymers. Note that 2 polymers deviate from the trend in recovery. More specifically, the first one is characterized by an exceptionally high acrylate content (2-3x higher) while the other corresponds with the highest molecular weight, allowing chain entanglements to play a more important role.

While no clear trend is found in fixity values of the different polymers, the recovery values correlate with the acrylate content of the polymers, with a higher acrylate content generally leading to improved recovery (Figure 6), a trend that has also been observed in literature and can be explained by the fact that polymers with a higher degree of crosslinking will be able to store more elastic strain energy and will thus result in higher recovery values.[40,41] Indeed, the entropy difference between the temporary shape and permanent shape will be the greatest for polymers with a lower molar mass between crosslinks and thus a higher crosslink density.[42] Therefore, a 4-armed star-shaped polymer of a similar molecular weight to a linear one can be expected to perform better with regard to shape-memory properties since its acrylate content will be higher for equal degrees of substitution. Two materials did not follow this trend, the first being 4-PDLLA/PCL6-2K-AUP which is characterized by an exceptionally high acrylate content compared with the other materials, the other being 2-PDLLA/PCL6-11K-AUP which has a higher R_r than expected based on the trend. However, since this material constitutes the highest molar mass per arm and is linear, the chain entanglements could potentially act as physical crosslinks, improving the recovery value of the material when the temporary shape is only held for a limited time and creep effects are minimal. The fact that chain entanglements can act as physical crosslinks was already shown for uncrosslinked high molecular weight

poly(ethylene), which also shows shape-memory behavior despite having no chemical nor physical crosslinks.[43] When comparing the obtained fixity and recovery values with literature, it becomes clear that these materials perform similar or better than previously described shape-memory materials based on PLA.[15,44–47] For example, Fan *et al*. have reported on a poly(PLLA/PDLLA-urethane) SMP which reaches R_f values of >99% and R_r values ranging between 75% and 99.7%, whereas our polymers shows comparable R_f values for most materials and R_r values approaching or outperforming those described in the state-of-the-art.[15] An example of a 4-PDLLA/PCL6-2K-AUP going through programming by heating to 37 °C, cooling to room temperature and fixing the shape to obtain the temporary shape and recovery by heating the temporary shape to 37 °C in a warm water bath is shown in Figure 7. Here, complete recovery of the sample was achieved within 1 s, which is relatively fast considering that other polymers reported in literature usually take > 5 s to recover their permanent shape, at best.[45,47] For example, a shape-memory polymer based on a PCL-PDLLA copolymer reported in literature took > 12 s to recover its permanent shape.[48]

Table 5. Overview of shape fixity and shape recovery values of the shape-memory materials

	Cycle 1		Cycle 3		Cycle 5	
Material	R_f [%]	R_r [%]	R_f [%]	R_r [%]	R_f [%]	R_r [%]
2-PDLLA/PCL6-11K-AUP	99.61	93.49	99.58	98.71	99.54	99.41
2-PDLLA/PCL6-7K-AUP	99.57	93.87	99.53	97.95	99.54	96.90
2-PDLLA/PCL6-9K-AUP	87.93	81.95	88.70	96.07	88.66	98.39
2-PDLLA/PCL8-8K-AUP	95.97	77.73	96.27	96.79	96.39	98.65
3-PDLLA-9K-AUP	96.42	90.86	96.83	98.32	96.82	99.38
4-PDLLA-12K-AUP	96.74	97.44	96.85	99.72	96.80	100
4-PDLLA/PCL6-2K-AUP	93.18	96.46	96.47	97.57	96.37	99.57

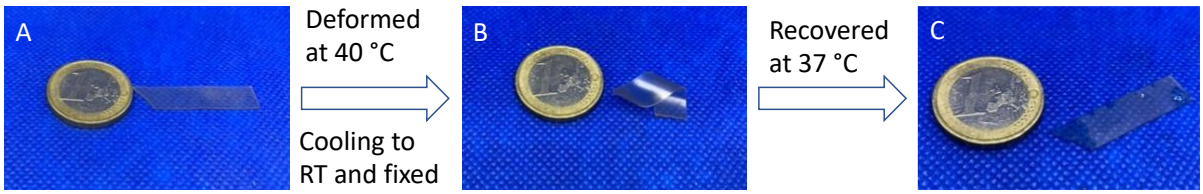

Figure 8. 4-PDLLA/PCL6-2K-AUP in its permanent shape (A) was heated, deformed and cooled down to fix the temporary shape. (B) Upon heating by immersing in a 37 °C water bath, the permanent shape is recovered (C).

4.6 Accelerated *in vitro* degradation assay

An accelerated degradation assay (1M NaOH, 37 °C) was performed on polymers that were crosslinkable crosslinking according to the rheological assessment (Figure 9). It was expected that more densely crosslinked polymer networks would show slower degradation rates, as previously reported in literature.[49]

However, the fastest degradation rates (complete degradation after 24h) were observed for polymers with a shorter backbone (4-PDLLA/PCL6-2K-AUP and 2-PDLLA/PCL6-4K-AUP),

and thus a more crosslinked network appears to degrade faster, despite the incorporation of ε-caprolactone, which is known to slow down hydrolytic degradation.[50] This can be attributed to the fact that polymers with a higher crosslink density will have a higher fraction of the hydrophilic PEG spacer incorporated within their matrix, increasing their hydrophilicity and hence accelerating their degradation. Indeed, when comparing the degradation rates of 3-PDLLA-9K-AUP and 4-PDLLA-12K-AUP, it is noticeable that the fastest degradation is observed for the polymer with a higher backbone molar mass. Even when considering the molar mass per arm, which is more or less equal (~3000 g/mol) for both polymers, the least branched backbone shows slower degradation. This can again be attributed to the OEG content as the 4-armed polymer displayed a slightly higher (0.34 mmol g^{-1}) endcap content compared to the 3-armed polymer (0.33 mmol g-1).

This leads to the conclusion that degradation rates will be higher for polymers with a lower molar mass per arm, due to their higher PEG content and thus higher hydrophilicity. The incorporation of the PEG spacer is thus the reason for the unexpected degradation behavior.[49] A similar conclusion has been made before for PEG-PLA block-copolymers, where polymers with a greater PEG content were found to degrade faster.[51]

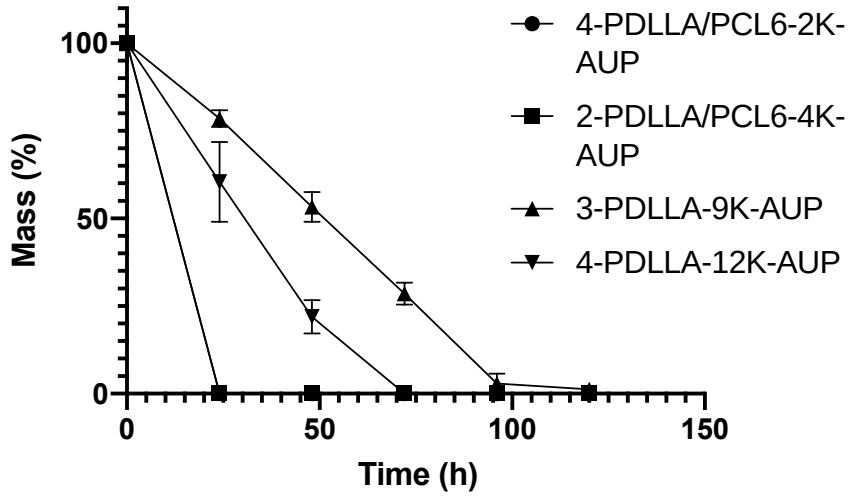

Figure 9. Accelerated degradation profiles of selected shape-memory polymers.

4.7. Cytocompatibility

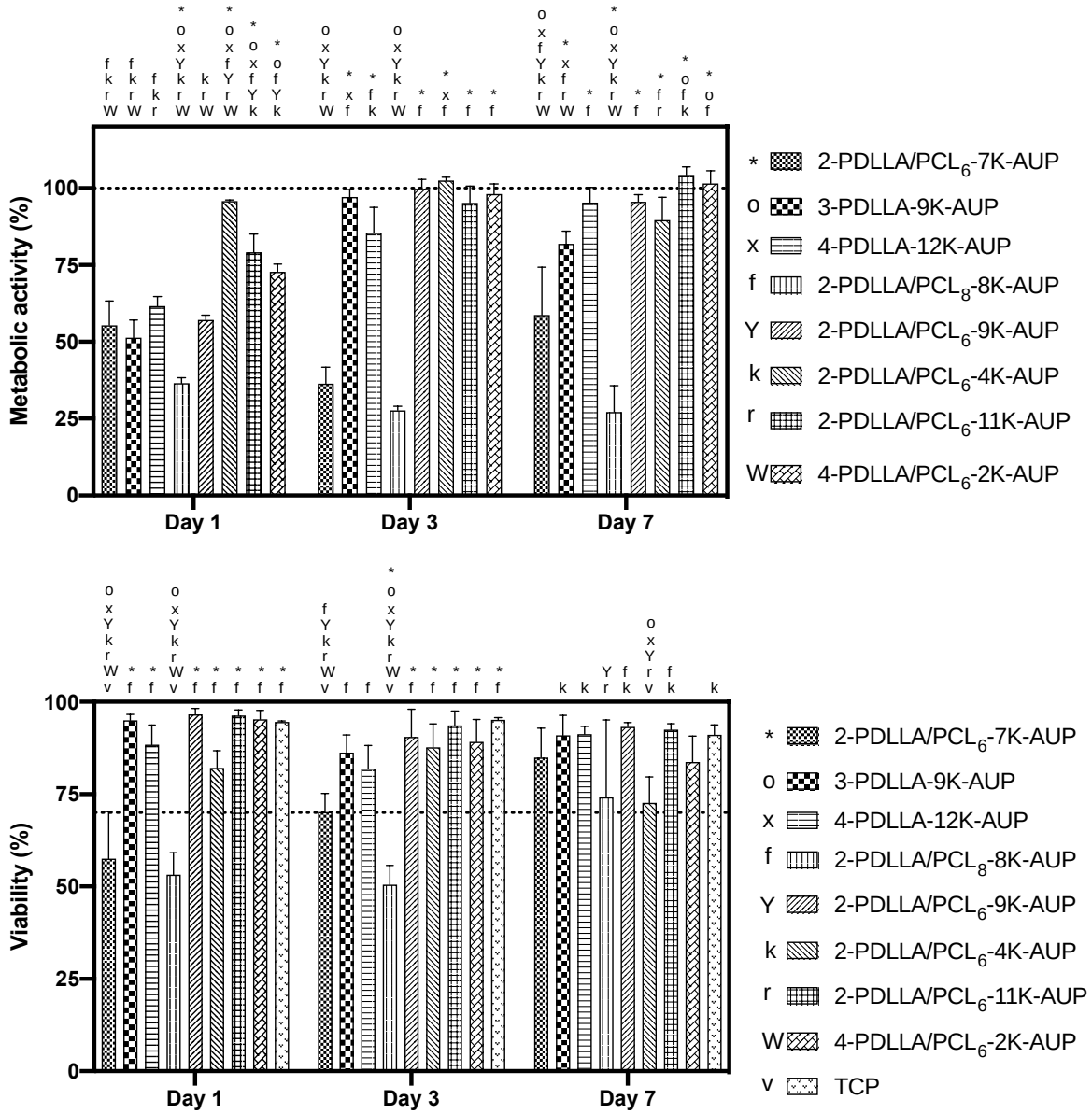

Figure 10. MTS metabolic activity assay (top) and cell viability (bottom) of the various shape-memory polymers. In the MTS assay, metabolic activity was determined relative to TCP (100%, dotted line). The dotted line in the bottom picture indicates the general level at which a material is considered to be biocompatible (i.e. 70% viability) Significances are indicated above each graph when a graphed material has a significant difference ($p \leq 0.05$) with the material with the corresponding symbol.

Metabolic activity (MTS assay) and cell viability (live-dead) were evaluated relative to tissue culture plastic (TCP) by means of a direct contact test using primary HFFs (Figure 10). In general, high viabilities were observed for all polymers, except for 2-PDLLA/PCL8-8K-AUP. Here, viability falls below the 70% mark at day 1 and 3. By day 7, all conditions corresponded with a cell viability exceeding 70% while most polymers even resulted in cell viabilities exceeding 90%. Only 2-PDLLA/PCL6-7K-AUP and 2-PDLLA/PCL8-8K-AUP performed significantly worse compared to TCP (84.9% and 74.2%, $p<0.05$ and $p<0.02$ respectively). When considering the metabolic activity, it is clear that by day 3, cells exposed to most polymers show relatively metabolic activity comparable to TCP, the exceptions being 2-

PDLLA/PCL6-7K-AUP and 2-PDLLA/PCL8-8K-AUP, which corresponded with lower viabilities, indicating a reduced proliferation of the cells in contact with these materials. The other materials on the other hand supported cell proliferation as reflected by the high cell viabilities and metabolic activities approaching or exceeding 100% relative to TCP. Especially 4-PDLLA-12K-AUP, 2-PDLLA/PCL6-4K-AUP, 2-PDLLA/PCL6-11K-AUP and 4-PDLLA/PCL6-2K-AUP performed well, with cells being of comparable metabolic activity to those in contact with other polymers or TCP at day 7. The latter combined with the high cell viability points towards excellent cell proliferation. For some polymers, a slight drop in metabolic activity and cell viability is observed at day 7, which is correlated with overcrowding of the cell environment but still maintaining relative metabolic activity values exceeding 80%. 2-PDLLA/PCL6-7K-AUP and especially 2-PDLLA/PCL8-8K-AUP seem to perform significantly worse. However, it needs to be considered that the assay medium of these polymers showed a slightly lowered pH which is most likely caused by the hydrolytic degradation of the PLA chains into lactic acid. It is likely that even these polymers would exhibit high viabilities in an *in vivo* context where lactic acid might be transported away from the cells. However, given the apparent rapid onset of degradation for these polymers, their usefulness in practical applications might be limited.
The excellent cytocompatibility of these polymers was anticipated given the fact that both AUP-type materials with different backbone chemistries[52,53] and P(DL)LA[54,55] have an excellent track record with regard to cytocompatibility.

4.7. Processing of the shape-memory AUPs

4.7.1 Digital light processing (DLP)

For DLP processing of the shape-memory polymers, a photo-crosslinkable resin was developed from 4-PDLLA/PCL6-2K-AUP, since this polymer exhibited the highest acrylate content and the highest storage modulus in the crosslinked state, making it more robust during the printing process. To this end, the polymer was dissolved in NMP (40 w V^{-1} %) to reduce the viscosity of the material to a workable state (< 3 Pa.s)[35]. The selected concentration coincides with the most concentrated solution that was achieved in this solvent while maintaining complete dissolution of the polymer. Additionally, NMP was selected as solvent since a high boiling point solvent (202 °C) is required for DLP printing to prevent evaporation of the solvent during printing which can otherwise result in deviations from the CAD model.[56] This made other good solvents for the polymers, such as acetone, chloroform or THF unsuitable. TPO-L (10 mol% with respect to the acrylates) was incorporated as photoinitiator based on its excellent cytocompatibility and good solubility in the selected solvent.[57] Additionally, the λ_{max} of TPO-L (383 nm)[58] is relatively close to the light emitted by the DLP device (405 nm), making initiation efficient and reducing curing times. The photoinitiator concentration was selected based upon complete gelation of the polymer solution after exposure to the DLP light source for 1s. Indeed, lower concentrations resulted in incomplete curing of the material or required longer curing times. Although the resin was printable, overcuring, as evidenced by the presence of cured material outside of the illuminated area, occurred which was especially noticeable near the base plate of the printer (see supplementary information). This was in line with previous results described in literature, where it was found that the addition of a photoabsorber is often needed to improve the resolution by limiting light penetration in the resin.[59,60] Therefore, Quinoline yellow (QY), which was already described in literature[59,61], was added

as a photoabsorber (0.5 mol% relative to the AUP double bonds). Since peak absorption of QY (412 nm) is close to the wavelength of the DLP light source (405 nm), QY was anticipated to provide excellent improvement regarding vertical resolution.[61] The resulting resin showed excellent printability (Figure 10A). After leaching of the residual solvent, the print shrunk considerably compared to the initial print. By calculating the degree of shrinkage, it becomes possible to predict the dimensions of the final print after solvent removal. The results showed that prints after leaching and drying were smaller as visualized in Figure 11. Additionally, the hardness of the print increased from a soft to a hard material, indicating successful removal of the solvent having a plasticizing effect, and used to create the formulation for DLP printing.

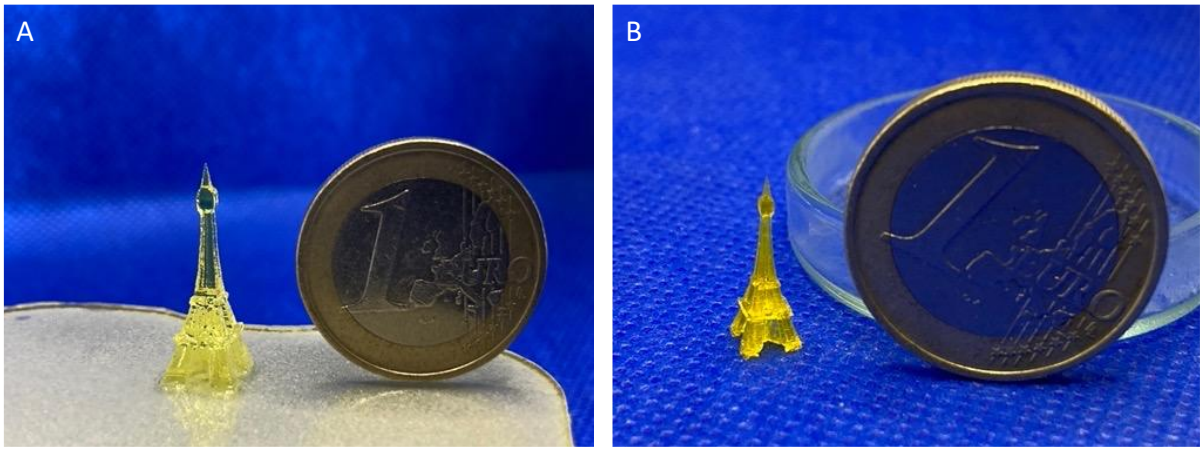

Figure 11. Printed tower before (A) and after (B) leaching of the solvent present in the resin.

Before leaching of the residual solvent, the 3D-printed construct did not exhibit shape-memory behavior due to the plasticizing effect of the solvent. After leaching, the shape-memory properties were demonstrated by heating the tower above the T_g (T_g + 5 °C) of the polymer material and allowing it to cool down to room temperature, fixating the temporary shape (Figure 12B). Upon reheating, the tower recovered its upright shape (Figure 12C), indicating that the DLP printing method is suitable for the processing of shape-memory resins. Moreover, with a recovery time of 15s, recovery occurred twice as fast compared to a recently reported polyester (Poly(1,2,3,6-Tetrahydrophthalic Anhydride-Co-Allyl Glycidol Ether)) resin exhibiting shape-memory properties.[62] The fixing of the temporary shape and the recovery of the polymer shape were repeated successfully over 5 times. However, there is no theoretical limit preventing more deformation and recovery cycles from occurring.

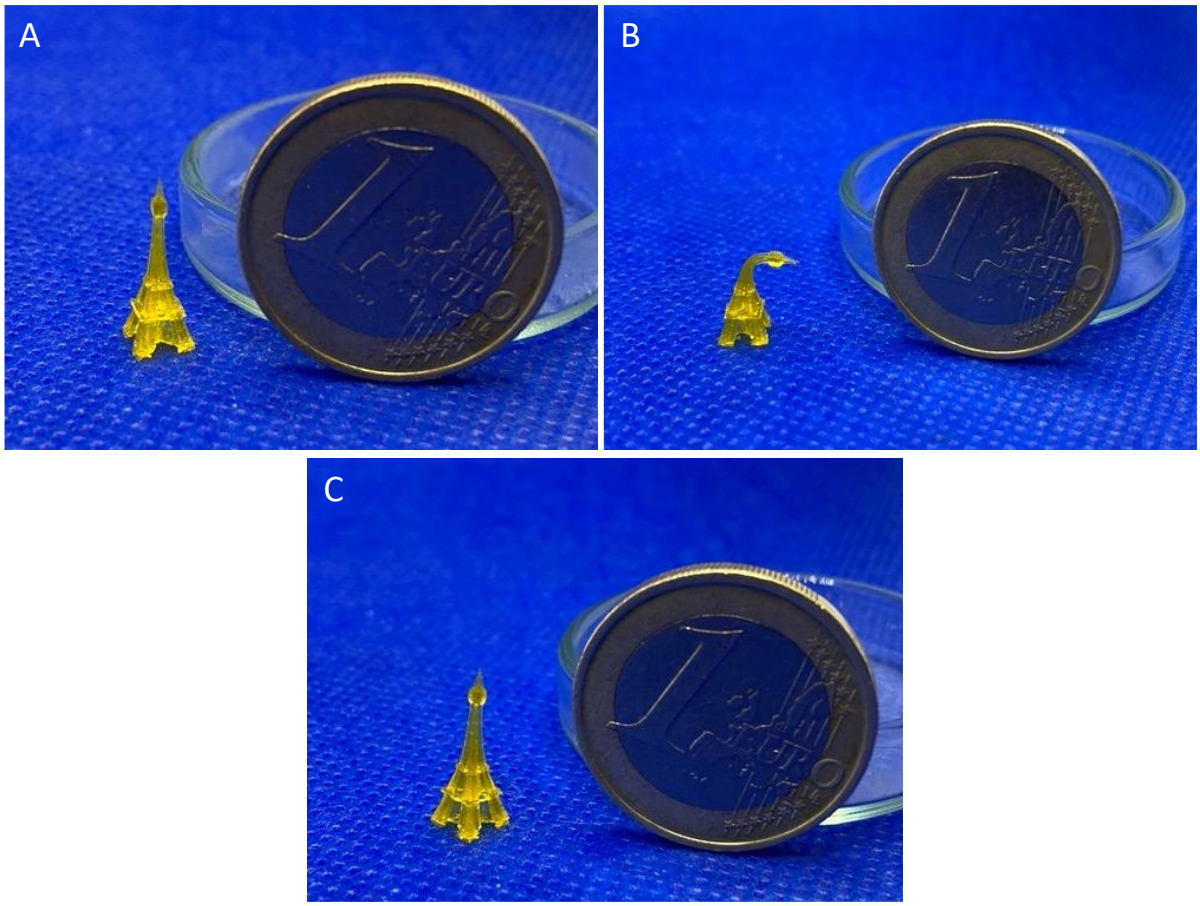

Figure 12. Demonstration of the shape-memory effect for a 3D printed tower. The initial shape (A) is deformed at elevated temperatures and cooled down to obtain the temporary shape (B). Reheating results in recovery of the original shape (C).

4.7.2. 2-photon polymerization (2PP)

2-photon polymerization was performed with 4-PDLLA/PCL6-2K-AUP because of its high acrylate content (0.91 mmol g^{-1}), using both a conventional photoinitiator (TPO-L)[63,64] and a 2-photon initiator (2PI) (M2CMK)[25,29,65]. Printability turned out to be excellent for both photoinitiators, while a lower concentration of the 2PI was needed (1 wt% instead of 5wt% of traditional PI) to achieve equivalent results. In addition, the printing speed could be significantly increased when exploiting a 2PI (i.e. a printing speed of 100 mm s^{-1} for the convention photoinitiator versus a printing speed of 600 mm s^{-1} for the 2PI). For both resins, the minimally required laser power was determined by printing an array of cubes at varying laser intensities (Figure 13). Here, discernable prints appeared for the conventional photoinitiator (100 mm s^{-1}) at 60 mW and for the 2PI at 20 and 30 mW for a printing speed of 100 mm s^{-1} and 600 mm s^{-1} respectively. For the printing of more complex constructs, this power was doubled to ensure sufficient crosslinking of the material.

In case of the conventional photoinitiator, a more complex structure was also printed. Interestingly, even when exploiting a conventional PI, the resolution turned out to be excellent and all features of the print were visible indicating a good CAD-CAM mimicry (Figure 13). This is remarkable, since earlier work reporting on linear AUP-PCL-based polymers showed

the need for the use of endcaps containing three acrylates instead of one to obtain a rigid structure with no distortion.[66]

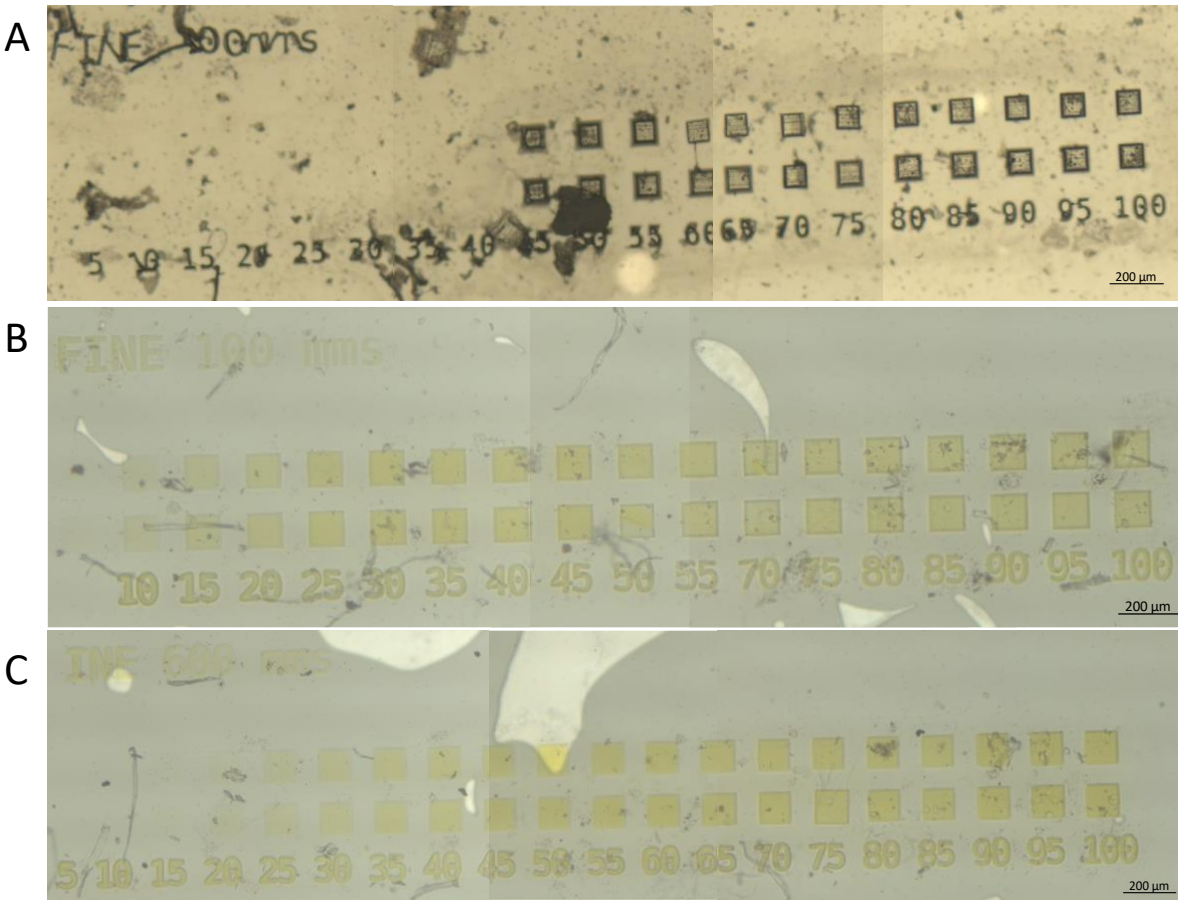

Figure 13. 2PP printing of 4-PDLLA/PCL6-2K-AUP using TPO-L as photoinitiator (A) and M2CMK as photoinitiator (B&C) at 100 mm s^{-1} (B) and 600 mm s^{-1} (C) at various laser powers. The laser power varied for printing of the cubes and is printed underneath the cubes in each image.

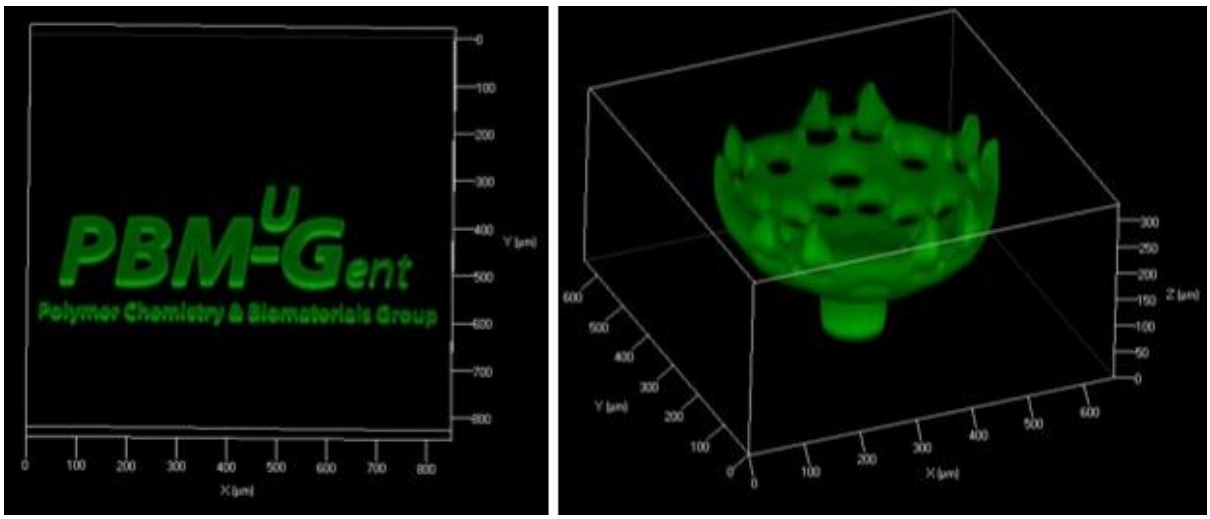

Figure 14. Confocal microscopy image of the group logo (left) and of a more complex 3D printed structure (right) using TPO-L as photoinitiator.

4.7.3. Direct powder extrusion (DPE)

DPE printing was performed using the 2-PDLLA/PCL6-9K-AUP which was pulverized and blended with 2 mol% of Irgacure 2959. This polymer was selected since it does not display any significant flow at room temperature, hence not requiring a cooled printing bed to print this material. Additionally, this polymer performed excellent in the gel fraction tests, indicating excellent crosslinking behavior. Due to the high viscosity of the polymer, an extrusion speed of 5 mm s^{-1} was selected combined with a relatively slow printing speed of 0.5 mm s^{-1}. Using higher printing speeds resulted in failure of the print to attach to the build plate while lower extrusion speeds resulted in non-continuous extrusion of the polymer, resulting in gaps in the print. A temperature of 65 °C was selected as extrusion temperature, this represented the lowest temperature at which printing was possible, lower temperatures resulted in the non-continuous extrusion of the polymer while higher temperatures did not result in any noticeable improvements in the print. An overview of the tested parameters and the selected optimums is shown in Table 6. After printing, the construct was crosslinked by irradiating the complete construct with UV-A light for 30 min and the shape-memory effect was qualitatively evaluated by heating the printed construct, changing its shape and observing the recovery of the deformed print when placed in warm water (40 °C) as shown in Figure 15. Recovery of the printed construct occurred over the course of 34s, which is much slower compared to the constructs printed using DLP. This slower recovery might be related to suboptimal crosslinking of the construct with the crosslinking efficiency decreasing in the inner parts of the extruded struts and layers due to the limited penetration depth of the UV light, this in contrast with DLP during which X-Y planes with a thickness of 50 μm are crosslinked through UV irradiation. Additionally, for DPE, Irgacure 2959 was used as a photoinitiator which has a λ_{max} of ~275 nm which does not overlap with the UV-A light ($\lambda = 300$-400 nm) that was used, resulting in suboptimal initiation. Another explanation could be the relatively lower acrylate content and crosslink density and the associated lower R_f and R_r values resulting in a less efficient and slower shape-memory effect in this material.

Table 6. Overview of printing parameters exploited in DPE

Property	Range tested	Optimum
Temperature	60-70 °C	65 °C
Layer height	0.4-0.6 mm	0.5 mm
Infill angle	N/A	90°
Flow speed	3-5 mm s-1	5 mm s-1
Retract speed	N/A	10 mm s-1
Perimeter/Skirt speed	0.5-2 mm s-1	0.5 mm s-1
Infill speed	0.5-2 mm s-1	0.5 mm s-1
Travel speed	N/A	20 mm s-1

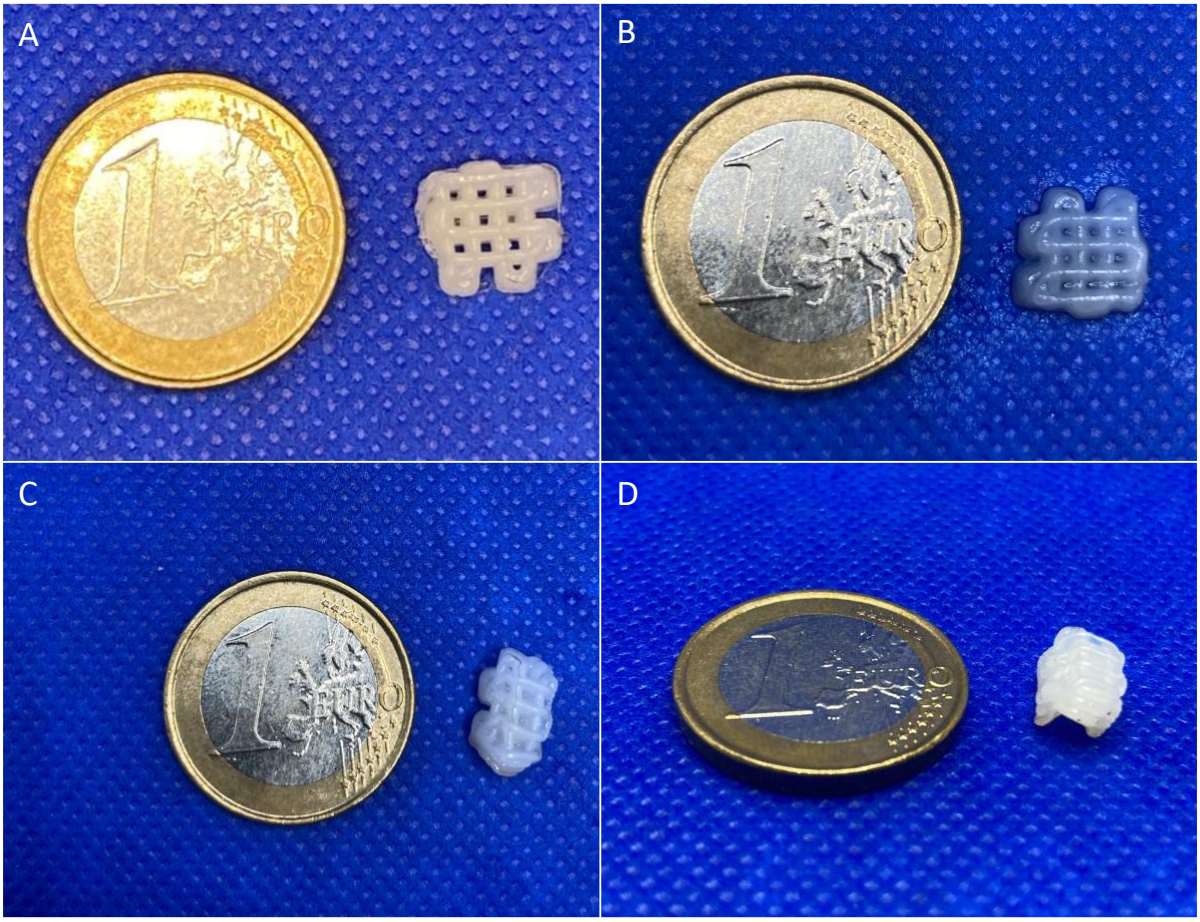

Figure 15. Overview of the permanent shape of the construct (A), the recovered permanent shape (B) and the temporary shape (C, D).

5. Conclusions

Various novel shape-memory polymers were developed based on AUP chemistry, varying the PDLLA/PCL (main chain mobility) content and acrylate content (crosslink density). These polymers were proven to have excellent shape-memory capabilities with excellent fixity and recovery values (> 99%), as well as fast recovery (2-15 s) with only the material processed using DPE showing slower recovery (34 s). The data indicated that star-shaped polymers exhibit improved shape-memory properties compared to their linear counterparts of similar molar mass. Moreover, since all polymers are amorphous, their shape-memory effect is based on the glass transition. Varying the ratio of PDLLA/PCL in the backbone allows for tuning of the glass transition temperature and hence, the shape-memory transition temperature. The glass transition temperature, and thus the shape transition temperature, of the crosslinked material was shown to be predictable by employing Fox' equation. It was concluded that a CL content of 6 wt% results in a polymer of which the glass transition temperature is ideal, being situated between room temperature and body temperature, hence ensuring transition of a potential implant upon implantation without risking premature transition at room temperature. Additionally, most polymers exhibited excellent cytocompatibility as reflected by the metabolic activity and viability of HFF cells upon direct contact with the developed shape-memory materials. Finally, a formulation of the 4-armed low molecular weight AUP 4-PDLLA/PCL6-2K-AUP to be applied in DLP processing was developed. The data showed that

the polymer proved to be 3D printable while retaining its shape-memory properties. Moreover, it was proven that the material was processible using 2PP in solid state, both with a conventional and a 2-photon photoinitiator. Here, resolution was shown to be excellent as reflected by the capability to print complex structures without issues and with good CAD-CAM mimicry. Lastly, processing of 2-PDLLA/PCL6-11K-AUP using an extrusion-based method followed by UV-crosslinking was proven while retaining the shape-memory properties.

6. Acknowledgements

J. Delaey would like to express their gratitude towards the Research Foundation Flanders (FWO) for their financial support during the project through grant number 1SA2121N. Additionally, the authors would like to thank the FWO for their support through project G059419N and G056219N.

References

[1] J. Delaey, P. Dubruel, S. Van Vlierberghe, *Adv. Funct. Mater.* **2020**, *1909047*, 1909047.
[2] M. C. Chen, H. W. Tsai, Y. Chang, W. Y. Lai, F. L. Mi, C. T. Liu, H. S. Wong, H. W. Sung, *Biomacromolecules* **2007**, *8*, 2774.
[3] E. Zini, M. Scandola, P. Dobrzynski, J. Kasperczyk, M. Bero, *Biomacromolecules* **2007**, *8*, 3661.
[4] M. Montgomery, S. Ahadian, L. Davenport Huyer, M. Lo Rito, R. A. Civitarese, R. D. Vanderlaan, J. Wu, L. A. Reis, A. Momen, S. Akbari, A. Pahnke, R.-K. Li, C. A. Caldarone, M. Radisic, *Nat. Mater.* **2017**, *16*, 1038.
[5] C. Wischke, A. T. Neffe, S. Steuer, A. Lendlein, *J. Control. Release* **2009**, *138*, 243.
[6] C. Wischke, A. T. Neffe, S. Steuer, E. Engelhardt, A. Lendlein, *Macromol. Biosci.* **2010**, *10*, 1063.
[7] G. Li, G. Fei, H. Xia, J. Han, Y. Zhao, *J. Mater. Chem.* **2012**, *22*, 7692.
[8] A. Toncheva, F. Khelifa, Y. Paint, M. Voué, P. Lambert, P. Dubois, J. M. Raquez, *ACS Appl. Mater. Interfaces* **2018**, *10*, 29933.
[9] M. Zarek, N. Mansour, S. Shapira, D. Cohn, *Macromol. Rapid Commun.* **2017**, *38*, 1.
[10] Y. Guo, Z. Lv, Y. Huo, L. Sun, S. Chen, Z. Liu, C. He, X. Bi, X. Fan, Z. You, *J. Mater. Chem. B* **2019**, *7*, 123.
[11] Y. Xiao, S. Zhou, L. Wang, T. Gong, *ACS Appl. Mater. Interfaces* **2010**, *2*, 3506.
[12] Y. C. Shin, J. B. Lee, D. Kim, T. Kim, G. Alexander, Y. M. Shin, J. Y. Park, S. Baek, J. Yoon, Y. J. Lee, G. M. Seon, M. H. Lee, M. Kang, W. S. Jang, J. Park, H. Jun, Y. Kim, H. Sung, *Adv. Mater.* **2019**, *31*, 1904476.
[13] J. Yang, F. Liu, L. Yang, S. Li, *Eur. Polym. J.* **2010**, *46*, 783.
[14] M. Bao, X. Lou, Q. Zhou, W. Dong, H. Yuan, Y. Zhang, *ACS Appl. Mater. Interfaces* **2014**, *6*, 2611.
[15] X. Fan, B. H. Tan, Z. Li, X. J. Loh, *ACS Sustain. Chem. Eng.* **2017**, *5*, 1217.
[16] H. Xie, M. J. He, X. Y. Deng, L. Du, C. J. Fan, K. K. Yang, Y. Z. Wang, *ACS Appl. Mater. Interfaces* **2016**, *8*, 9431.
[17] A. Lendlein, R. Langer, *Science* **2002**, *296*, 1673.
[18] A. Garle, S. Kong, U. Ojha, B. M. Budhlall, *ACS Appl. Mater. Interfaces* **2012**, *4*, 645.
[19] L. Wang, X. Yang, H. Chen, T. Gong, W. Li, G. Yang, S. Zhou, *ACS Appl. Mater. Interfaces* **2013**, *5*, 10520.
[20] X. L. Lu, W. Cai, Z. Gao, W. J. Tang, *Polym. Bull.* **2007**, *58*, 381.
[21] M. Balk, M. Behl, C. Wischke, J. Zotzmann, A. Lendlein, *Adv. Drug Deliv. Rev.* **2016**, *107*, 136.
[22] M. Hiljanen-Vainio, T. Karjalainen, J. Seppälä, *J. Appl. Polym. Sci.* **1996**, *59*, 1281.
[23] A. Houben, P. Roose, H. Van den Bergen, H. Declercq, J. Van Hoorick, P. Gruber, A. Ovsianikov, D. Bontinck, S. Van Vlierberghe, P. Dubruel, *Mater. Today Chem.* **2017**, *4*, 84.
[24] P. Dubruel, S. Van Vlierberghe, A. Houben, H. Van den Bergen, P. Roose, D. Bontinck, Novel urethane based materials, derivatives, methods of their preparation and uses **2017**, 44.
[25] Z. Li, N. Pucher, K. Cicha, J. Torgersen, S. C. Ligon, A. Ajami, W. Husinsky, A. Rosspeintner, E. Vauthey, S. Naumov, T. Scherzer, J. Stampfl, R. Liska, *Macromolecules* **2013**, *46*, 352.
[26] P. J. Flory, *Principles of Polymer Chemistry*; Cornell Universtiy Press: Ithaca, N.Y., 1953.
[27] T. Chen, Characterization of shape memory polymers by DMA 1.
[28] T. Sauter, M. Heuchel, K. Kratz, A. Lendlein, *Polym. Rev.* **2013**, *53*, 6.
[29] A. Ajami, W. Husinsky, M. Tromayer, P. Gruber, R. Liska, A. Ovsianikov, *Appl. Phys. Lett.* **2017**, *111*.
[30] L. S. Nair, C. T. Laurencin, *Prog. Polym. Sci.* **2007**, *32*, 762.
[31] M. R. Nabid, S. J. Tabatabaei Rezaei, R. Sedghi, H. Niknejad, A. A. Entezami, H. A. Oskooie, M. M. Heravi, *Polymer (Guildf).* **2011**, *52*, 2799.
[32] S. H. Kim, Y.-K. Han, K.-D. Ahn, Y. H. Kim, T. Chang, *Macromol. Chem. Phys.* **1993**, *194*, 3229.

[33] P. J. Flory, J. Rehner, *J. Chem. Phys.* **1943**, *11*, 521.
[34] C. M. Yakacki, R. Shandas, C. Lanning, B. Rech, A. Eckstein, K. Gall, *Biomaterials* **2007**, *28*, 2255.
[35] M. Krkobabić, D. Medarević, N. Pešić, D. Vasiljević, B. Ivković, S. Ibrić, *Pharmaceutics* **2020**, *12*, 1.
[36] S. Rimdusit, W. Bangsen, P. Kasemsiri, *J. Appl. Polym. Sci.* **2011**, *121*, 3669.
[37] N. R. Richbourg, M. Wancura, A. E. Gilchrist, S. Toubbeh, B. A. C. Harley, E. Cosgriff-Hernandez, N. A. Peppas, *Sci. Adv.* **2021**, *7*.
[38] J. Shen, X. Lin, J. Liu, X. Li, *Macromolecules* **2019**, *52*, 121.
[39] C. Serra, *Free Radical Polymerization*; American Chemical Society Division of Polymeric Materials: Science and Engineering, 2013; Vol. 2.
[40] X. L. Wu, S. F. Kang, X. J. Xu, F. Xiao, X. L. Ge, *J. Appl. Polym. Sci.* **2014**, *131*, n/a.
[41] T. Calvo-Correas, N. Gabilondo, A. Alonso-Varona, T. Palomares, M. A. Corcuera, A. Eceiza, *Eur. Polym. J.* **2016**, *78*, 253.
[42] C. C. Hornat, M. W. Urban, *Prog. Polym. Sci.* **2020**, *102*, 101208.
[43] S. Kaloshkin, A. Maksimkin, M. Kaloshkina, M. Zadorozhnyy, M. Churyukanova, *MRS Proc.* **2012**, *1403*, mrsf11.
[44] J. Karger Kocsis, S. Siengchin, *Shape Memory Systems with Biodegradable Polyesters*; 2015.
[45] M. Behl, A. Lendlein, *Mater. Today* **2007**, *10*, 20.
[46] H. Wu, P. Chen, C. Yan, C. Cai, Y. Shi, *Mater. Des.* **2019**, *171*, 107704.
[47] A. Alteheld, Y. Feng, S. Kelch, A. Lendlein, *Angew. Chemie - Int. Ed.* **2005**, *44*, 1188.
[48] X. Yu, L. Wang, M. Huang, T. Gong, W. Li, Y. Cao, D. Ji, P. Wang, J. Wang, S. Zhou, *J. Mater. Sci. Mater. Med.* **2012**, *23*, 581.
[49] K. A. George, T. V. Chirila, E. Wentrup-Byrne, *Polym. Degrad. Stab.* **2012**, *97*, 964.
[50] V. Barral, S. Dropsit, A. Cayla, C. Campagne, É. Devaux, *Polymers (Basel).* **2021**, *13*, 1.
[51] Y. Wang, S. Zhang, D. S. W. Benoit, *J. Control. Release* **2018**, *287*, 58.
[52] A. Houben, N. Pien, X. Lu, F. Bisi, J. Van Hoorick, M. N. Boone, P. Roose, H. Van den Bergen, D. Bontinck, T. Bowden, P. Dubruel, S. Van Vlierberghe, *Macromol. Biosci.* **2016**, *16*, 1883.
[53] N. Pien, I. Peeters, L. Deconinck, L. Van Damme, L. De Wilde, A. Martens, S. Van Vlierberghe, P. Dubruel, A. Mignon, *Mater. Sci. Eng. C* **2021**, *119*, 111504.
[54] D. da Silva, M. Kaduri, M. Poley, O. Adir, N. Krinsky, J. Shainsky-Roitman, A. Schroeder, *Chem. Eng. J.* **2018**, *340*, 9.
[55] R. Y. Li, Z. G. Liu, H. Q. Liu, L. Chen, J. F. Liu, Y. H. Pan, *Am. J. Transl. Res.* **2015**, *7*, 1357.
[56] G. Varghese, M. Moral, M. Castro-García, J. J. López-López, J. R. Marín-Rueda, V. Yagüe-Alcaraz, L. Hernández-Afonso, J. C. Ruiz-Morales, J. Canales-Vázquez, *Boletín la Soc. Española Cerámica y Vidr.* **2018**, *57*, 9.
[57] G. T. Kim, H. Bin Go, J. H. Yu, S. Y. Yang, K. M. Kim, S. H. Choi, J. S. Kwon, *Polymers (Basel).* **2022**, *14*.
[58] C. Dietlin, T. T. Trinh, S. Schweizer, B. Graff, F. Morlet-Savary, P. A. Noirot, J. Lalevée, *Molecules* **2020**, *25*, 1.
[59] R. Zhang, N. B. Larsen, *Lab Chip* **2017**, *17*, 4273.
[60] J. W. Seo, G. M. Kim, Y. Choi, J. M. Cha, H. Bae, *Int. J. Mol. Sci.* **2022**, *23*.
[61] N. Anandakrishnan, H. Ye, Z. Guo, Z. Chen, K. I. Mentkowski, J. K. Lang, N. Rajabian, S. T. Andreadis, Z. Ma, J. A. Spernyak, J. F. Lovell, D. Wang, J. Xia, C. Zhou, R. Zhao, *Adv. Healthc. Mater.* **2021**, *10*, 1.
[62] D. Merckle, E. Constant, Z. Cartwright, A. C. Weems, *Macromolecules* **2021**, *54*, 2681.
[63] C. R. Mendonca, D. S. Correa, T. Baldacchini, P. Tayalia, E. Mazur, *Appl. Phys. A Mater. Sci. Process.* **2008**, *90*, 633.
[64] P. M. Cônsoli, A. J. G. Otuka, D. T. Balogh, C. R. Mendonça, *J. Polym. Sci. Part B Polym. Phys.* **2018**, *56*, 1158.
[65] A. Arslan, K. Vanmol, A. Dobos, A. Natale, J. Van Hoorick, P. Roose, H. Van Den Bergen, T. Chalyan, A. Ovsianikov, S. Baudis, V. Rogiers, T. Vanhaecke, R. M. Rodrigues, H. Thienpont, J. Van Erps, S. Van Vlierberghe, P. Dubruel, *Biomacromolecules* **2021**, *22*, 4919.
[66] A. Arslan, W. Steiger, P. Roose, H. Van den Bergen, P. Gruber, E. Zerobin, F. Gantner, O. Guillaume, A. Ovsianikov, S. Van Vlierberghe, P. Dubruel, *Mater. Today* **2021**, *44*, 25.